Figure 5. Effect of PKD inhibition in mice. A, PKD-mediated phosphorylation in the liver in doxazosin (Dox)-treated C57BL/6 mice (n=3 for each group). B, C, and D, Gö6983 or vehicle (C) was given to the mice (n=7 for each group). Liver protein (750 μg) immunoprecipitated with anti-AP2α antibody was analyzed with antibodies against phospho-Ser (pSer) and AP2α (Ap2) (B). Liver protein (5 μg) was analyzed by Western blotting with antibodies against phospho-PKD (pPKD) and PKD (C), and phospho-PKCα (pPKCα), PKCα, and phospho-PKC substrate (pPKC-substrate) (D). E, Expression of SREBP1 and SREBP2 in the liver and SREBP1 in the adipose tissue by measuring mRNA. The graphs represent quantified blotting data of at least 3 experiments. *P<0.05 and **P< 0.01.

Figure 6. Effect of PKD inhibition by Gö6983 in mouse. A, Expression of ABCA1 in the liver. Total RNA (50 ng) from the liver tissue (30 mg wet weight) was used for ABCA1 mRNA, and 50 μg protein was analyzed by Western blotting for ABCA1 protein. B, Plasma lipoprotein. Blood plasma was analyzed for lipoproteins by HPLC by monitoring total (TC) and free (FC) cholesterol, choline-phospholipids (PL), and triacylglycerol (TG). *P<0.05 and **P< 0.01.

Discussion

ABCA1 is a rate-limiting factor of plasma HDL level as it "catalyzes" HDL biogenesis.[26] This is an important part of body and cellular cholesterol homeostasis because cholesterol is not catabolized in extrahepatic peripheral cells except for steroidogenesis and therefore transported to the liver by HDL for conversion to bile acids.[26] This view is consistent with clinical findings that HDL is an apparent negative risk factor for atherosclerosis. Accordingly, increase of the ABCA1 activity may be an effective approach for prevention and cure of atherosclerosis. In the present study, we investigated molecular mechanism for negative regulation of ABCA1 gene expression by AP2α, expecting that this reaction may be a good pharmacological target for the increase of HDL biogenesis.

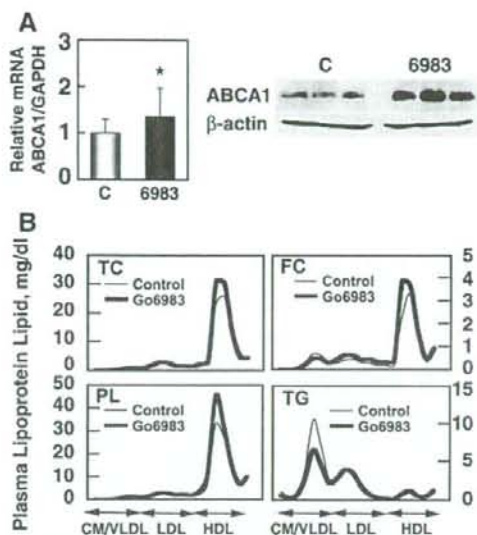Based on our finding that Ser-phosphorylation of AP2α was associated with its binding activity to the ABCA1 promoter,[1] potential sites for Ser-phosphorylation was analyzed in AP2α protein. Phosphorylation by PKD mainly at Ser258 was found related to the DNA binding activity of AP2α. The results are consistent with the previous findings that the region of this residue is included in the highly conserved basic domain of AP2α considered responsible for the binding to DNA after the dimerization mediated by the helix-span-helix domain.[4,5] From the results, however, minor involvement of Ser326 has not been excluded.

Doxazosin reduced phosphorylation of this specific site, decreased binding of AP2α to the ABCA1 promoter, and increased its transcription. Direct inhibition of PKD expression by siRNA resulted in the increase of ABCA1 expression and of biogenesis of HDL. Pharmacological inhibition of PKD also increased ABCA1 expression and its activity. Several mechanisms were proposed for posttranscriptional regulation of AP2α activity in previous reports, such as PKA-mediated phosphorylation,[2] redox regulation,[27] and sumoylation.[28] Physical interaction with various proteins was also indicated for modulation of the AP2α activity.[5] However, this study demonstrated that phosphorylation of a specific site(s) by PKD modulates AP2 binding to a specific site of DNA and its functional activity. PKA-phosphorylation was not investigated in detail in the present study, as PKA-phosphorylation did not seem affected by doxazosin. Also, it was previously shown that PKA-phosphorylation at Ser-239 does not influence DNA-binding of AP2α.[2] In addition, cAMP and therefore PKA activation has been indicated for ABCA1 upregulation rather than downregulation. Therefore, it is very unlikely that the Ser-239 phosphor-

ylation is involved in negative regulation of ABCA1 transcription via PKD/AP2α pathway. However, additional studies focusing on specific PKA-phosphorylation sites and ABCA1 expression should be required for complete exclusion of its involvement.

PKD was initially identified as a novel PKC-related enzyme PKCμ,[29] and later recognized as a new family of protein kinase. Its catalytic domain is not exactly similar to the conserved kinase domain of other PKC members but rather resembles that of calcium/calmodulin dependent kinases.[30] Many mediators to activate PKC also activate PKD, such as PMA, DAG, PDGF, oxdative stress, and several GPCR ligands (thrombin, serotonin, bradykinin, and lyso-phosphatidic acid).[9–12,31] It has recently been reported that PKD is activated by its phosphorylation of Ser744 and Ser748 mainly by PKC as it is blocked by PKC inhibitors including Gö6983.[25] It is interesting that Gö6983 more effectively inhibited PKD reaction than PKC-mediated reactions in cells and in vivo, in comparison to other compounds, in spite of the fact that its inhibitory activity is much stronger against PKC than against PKD.[32] We therefore chose Gö6983 for selective inhibition of PKD for this empirical reason. This compound in fact reproduced the effects of doxazosin in mice to increase ABCA1 expression and plasma HDL (Figure 6 and supplemental Table I).

PKD may also be involved in negative regulation of the adiponectin gene by AP2β,[6] as LRRAKS motif is conserved for AP2α and AP2β in their DNA binding domain. Overexpression of AP2β caused lipid accumulation and cellular enlargement in adipocytes.[6] Being consistent with these findings, our preliminary experimental observation showed that knockdown of PKD by siRNAs increased adiponectin mRNA in NIH3T3-L1 adipocytes and transcriptional activity of its promoter. PKD knockdown in the adipocyte decreased lipid droplet size shown by oil red O staining. Finally, PKD inhibition by Gö6983 in vivo resulted in increase of mRNA and plasma level of adiponectin. Lipid accumulation of adipocytes was decreased by the PKD knockdown.

PKD siRNA decreased SREBP1, an adipogenesis-regulating gene, but not SREBP2, a cholesterol homeostasis-regulating gene (Iwamoto et al, 2008 unpublished data). Inhibition of PKD by Gö6983 in vivo significantly diminished SREBP1 expression in the liver (Figure 5E) and presumably caused reduction of plasma triglyceride in mice (supplemental Table). A more recent report that inhibition of PKD increases release of lipoprotein lipase by cardiomyocytes may be consistent with these findings.[33]

PKD mediates mitogenic response to various growth factors, and potentiated cellular DNA synthesis by increasing duration of MEK/ERK/RSK signaling.[13,34] Furthermore, PKD enhanced antiapoptotic genes by activation of NF-κB through the IKB degradation in response to oxidative stress–PKD was required for cellular survival after oxdative stress–induced apoptosis.[31] Several other reports showed that doxazosin downregulated NF-κB signaling and induced apoptosis in some types of cells.[35–37] These findings are not inconsistent with our results of inhibition of PKD and AP2α phosphorylation by doxazosin.

Function of AP2 was generally related to cell proliferation, differentiation, and apoptosis. Fibroblast derived from AP2α-deficient mouse exhibited growth-retardation indicating its requirement for cell proliferation perhaps by suppressing the genes for terminal differentiation, apoptosis, and growth retardation.[15] Increased AP2 levels have been shown in various types of cancer cells.[16,17,38] The proto-oncogene c-erb-B2 expression has been reported regulated by AP2.[18] Among various subtypes of AP2, PKD recognition sites are well conserved. PKD knock-down by siRNA in HeLa cells decreased c-erb-B2 mRNA expression and cell proliferation rate (Iwamoto et al, 2008 unpublished data). Thus, PKD/AP2 signaling could regulate the balance of cell growth. During proliferation, cholesterol is required for cells to generate new membrane, and ABCA1 should perhaps be downregulated to prevent cholesterol from wasteful release. Therefore, action of AP2α on expression of the ABCA1 gene and HDL biogenesis may be consistent with other general function of this transcription factor for enhancing cell proliferation. In agreement with this view, PDGF reportedly increases 3-hydroxy-3-methylglutaryl (HMG)-coenzyme A (CoA) synthesis[39] and low-density lipoprotein receptor activity,[40] and decreases ABCA1 expression level.[41] Inhibition of cellular cholesterol biosynthesis by statins reduces proliferation of cancer cells.[42] It is also consistent with the finding that cellular free cholesterol doubled following the S-phase, and reached its maximum well before mitosis[43] by the increase of its uptake from extracellular lipoproteins and by the reduction of its release.

The potential scheme achieved by inhibition of the PKD/AP2 pathway is illustrated in supplemental Figure IV. This process would increase ABCA1, HDL, and adiponection and improve such multiple risk status defined as "metabolic syndrome." A question remains regarding what is a trigger for PKD/AP2α signal for regulation of the ABCA1 gene expression. Further investigation is needed to address this question, perhaps in the relation to regulation of cell growth.

In conclusion, we demonstrated that PKD phosphorylates Ser258 of AP2α and increases the DNA binding of AP2α protein. Inhibition of PKD/AP2α signaling pathway therefore decreases repression of the ABCA1 gene expression and accordingly increases ABCA1 and biogenesis of HDL. This finding is consistent with the other AP2-regulated gene, adiponectin. Inhibition of PKD thus would be a new drug target for prevention of atherosclerosis.

Source of Funding

Disclosures

Shinji Yokoyama is involved in the establishment of a venture company, HYKES Laboratories.

References

1. Iwamoto N, Abe-Dohmae S, Ayaori M, Tanaka N, Kusuhara M, Ohsuzu F, Yokoyama S. ATP-binding cassette transporter A1 gene transcription is downregulated by activator protein 2alpha. Doxazosin inhibits activator protein 2alpha and increases high-density lipoprotein

biogenesis independent of alpha1-adrenoceptor blockade. *Circ Res.* 2007;101:156–165.

2. Garcia MA, Campillos M, Marina A, Valdivieso F, Vazquez J. Transcription factor AP-2 activity is modulated by protein kinase A-mediated phosphorylation. *FEBS Lett.* 1999;444:27–31.

3. Nishikawa K, Toker A, Johannes FJ, Songyang Z, Cantley LC. Determination of the specific substrate sequence motifs of protein kinase C isozymes. *J Biol Chem.* 1997;272:952–960.

4. Williams T, Tjian R. Characterization of a dimerization motif in AP-2 and its function in heterologous DNA-binding proteins. *Science.* 1991;251: 1067–1071.

5. Eckert D, Buhl S, Weber S, Jager R, Schorle H. The AP-2 family of transcription factors. *Genome Biol.* 2005;6:246.1–246.8.

6. Ikeda K, Maegawa H, Ugi S, Tao Y, Nishio Y, Tsukada S, Maeda S, Kashiwagi A. Transcription factor activating enhancer-binding protein-2beta. A negative regulator of adiponectin gene expression. *J Biol Chem.* 2006;281:31245–31253.

7. Rozengurt E, Rey O, Waldron RT. Protein kinase D signaling. *J Biol Chem.* 2005;280:13205–13208.

8. Wang QJ. PKD at the crossroads of DAG and PKC signaling. *Trends Pharmacol Sci.* 2006;27:317–323.

9. Valverde AM, Sinnett-Smith J, Van Lint J, Rozengurt E. Molecular cloning and characterization of protein kinase D: a target for diacylglycerol and phorbol esters with a distinctive catalytic domain. *Proc Natl Acad Sci U S A.* 1994;91:8572–8576.

10. Zugaza JL, Waldron RT, Sinnett-Smith J, Rozengurt E. Bombesin, vasopressin, endothelin, bradykinin, and platelet-derived growth factor rapidly activate protein kinase D through a protein kinase C-dependent signal transduction pathway. *J Biol Chem.* 1997;272:23952–23960.

11. Tan M, Xu X, Ohba M, Ogawa W, Cui MZ. Thrombin rapidly induces protein kinase D phosphorylation, and protein kinase C delta mediates the activation. *J Biol Chem.* 2003;278:2824–2828.

12. Yuan J, Slice LW, Gu J, Rozengurt E. Cooperation of Gq, Gi, and G12/13 in protein kinase D activation and phosphorylation induced by lysophosphatidic acid. *J Biol Chem.* 2003;278:4882–4891.

13. Zhukova E, Sinnett-Smith J, Rozengurt E. Protein kinase D potentiates DNA synthesis and cell proliferation induced by bombesin, vasopressin, or phorbol esters in Swiss 3T3 cells. *J Biol Chem.* 2001;276: 40298–40305.

14. Wang Y, Waldron RT, Dhaka A, Patel A, Riley MM, Rozengurt E, Colicelli J. The RAS effector RIN1 directly competes with RAF and is regulated by 14-3-3 proteins. *Mol Cell Biol.* 2002;22:916–926.

15. Pfisterer P, Ehlermann J, Hegen M, Schorle H. A subtractive gene expression screen suggests a role of transcription factor AP-2 alpha in control of proliferation and differentiation. *J Biol Chem.* 2002;277: 6637–6644.

16. Turner BC, Zhang J, Gumbs AA, Maher MG, Kaplan L, Carter D, Glazer PM, Hurst HC, Haffty BG, Williams T. Expression of AP-2 transcription factors in human breast cancer correlates with the regulation of multiple growth factor signalling pathways. *Cancer Res.* 1998;58:5466–5472.

17. Hoei-Hansen CE, Nielsen JE, Almstrup K, Sonne SB, Graem N, Skakkebaek NE, Leffers H, Rajpert-De Meyts E. Transcription factor AP-2gamma is a developmentally regulated marker of testicular carcinoma in situ and germ cell tumors. *Clin Cancer Res.* 2004;10: 8521–8530.

18. Bosher JM, Totty NF, Hsuan JJ, Williams T, Hurst HC. A family of AP-2 proteins regulates c-erbB-2 expression in mammary carcinoma. *Oncogene.* 1996;13:1701–1707.

19. Hu W, Abe-Dohmae S, Tsujita M, Iwamoto N, Ogikubo O, Otsuka T, Kumon Y, Yokoyama S. Biogenesis of HDL by SAA is dependent on ABCA1 in the liver in vivo. *J Lipid Res.* 2008;49:386–393.

20. Yokoyama S, Tajima S, Yamamoto A. The process of dissolving apolipoprotein A-I in an aqueous buffer. *J Biochem (Tokyo).* 1982;91: 1267–1272.

21. Buettner R, Kannan P, Imhof A, Bauer R, Yim SO, Glockshuber R, Van Dyke MW, Tainsky MA. An alternatively spliced mRNA from the AP-2 gene encodes a negative regulator of transcriptional activation by AP-2. *Mol Cell Biol.* 1993;13:4174–4185.

22. Williams T, Admon A, Luscher B, Tjian R. Cloning and expression of AP-2, a cell-type-specific transcription factor that activates inducible enhancer elements. *Genes Dev.* 1988;2:1557–1569.

23. Zugaza JL, Sinnett-Smith J, Van Lint J, Rozengurt E. Protein kinase D (PKD) activation in intact cells through a protein kinase C-dependent signal transducation pathway. *EMBO J.* 1996;15:6220–6230.

24. Rykx A, De Kimpe L, Mikhalap S, Vantus T, Seufferlein T, Vandenheede JR, Van Lint J. Protein kinase D: a family affair. *FEBS Lett.* 2003;546:81–86.

25. Jacamo R, Sinnett-Smith J, Rey O, Waldron RT, Rozengurt E. Sequential PKC-dependent and PKC-independent protein kinase D catalytic activation via Gq-coupled receptors: Differential regulation of activation loop Ser744 and Ser748 phosphorylation. *J Biol Chem.* 2008;283:12877–12887.

26. Yokoyama S. Assembly of high-density lipoprotein. *Arterioscler Thromb Vasc Biol.* 2006;26:20–27.

27. Huang Y, Domann FE. Redox modulation of AP-2 DNA binding activity in vitro. *Biochem Biophys Res Commun.* 1998;249:307–312.

28. Eloranta JJ, Hurst HC. Transcription factor AP-2 interacts with the SUMO-conjugating enzyme UBC9 and is sumolated in vivo. *J Biol Chem.* 2002;277:30798–30804.

29. Johannes FJ, Prestle J, Eis S, Oberhagemann P, Pfizenmaier K. PKCu is a novel, atypical member of the protein kinase C family. *J Biol Chem.* 1994;269:6140–6148.

30. Manning G, Whyte DB, Martinez R, Hunter T, Sudarsanam S. The protein kinase complement of the human genome. *Science.* 2002;298: 1912–1934.

31. Storz P, Toker A. Protein kinase D mediates a stress-induced NF-kappaB activation and survival pathway. *EMBO J.* 2003;22: 109–120.

32. Gschwendt M, Dieterich S, Rennecke J, Kittstein W, Mueller HJ, Johannes FJ. Inhibition of protein kinase C mu by various inhibitors. Differentiation from protein kinase c isoenzymes. *FEBS Lett.* 1996; 392:77–80.

33. Kim MS, Wang F, Puthanveetil P, Kewalramani G, Hosseini-Beheshti E, Ng N, Wang Y, Kumar U, Innis S, Proud CG, Abrahani A, Rodrigues B. Protein kinase D is a key regulator of cardiomyocyte lipoprotein lipase secretion after diabetes. *Circ Res.* 2008;103:252–256.

34. Sinnett-Smith J, Zhukova E, Hsieh N, Jiang X, Rozengurt E. Protein kinase D potentiates DNA synthesis induced by Gq-coupled receptors by increasing the duration of ERK signaling in swiss 3T3 cells. *J Biol Chem.* 2004;279:16883–16893.

35. Fernando MA, Heaney AP. Alpha1-adrenergic receptor antagonists: novel therapy for pituitary adenomas. *Mol Endocrinol.* 2005;19: 3085–3096.

36. Gonzalez-Juanatey JR, Iglesias MJ, Alcaide C, Pineiro R, Lago F. Doxazosin induces apoptosis in cardiomyocytes cultured in vitro by a mechanism that is independent of alpha1-adrenergic blockade. *Circulation.* 2003;107:127–131.

37. Benning CM, Kyprianou N. Quinazoline-derived alpha1-adrenoceptor antagonists induce prostate cancer cell apoptosis via an alpha1-adrenoceptor-independent action. *Cancer Res.* 2002;62:597–602.

38. Bar-Eli M. Gene regulation in melanoma progression by the AP-2 transcription factor. *Pigment Cell Res.* 2001;14:78–85.

39. Roth M, Emmons LR, Perruchoud A, Block LH. Expressions of the low density lipoprotein receptor and 3-hydroxy-3-methylglutaryl coenzyme A reductase genes are stimulated by recombinant platelet-derived growth factor isomers. *Proc Natl Acad Sci U S A.* 1991;88:1888–1892.

40. Witte LD, Cornicelli JA. Platelet-derived growth factor stimulates low density lipoprotein receptor activity in cultured human fibroblasts. *Proc Natl Acad Sci U S A.* 1980;77:5962–5966.

41. Nagao S, Murao K, Imachi H, Cao WM, Yu X, Li J, Matsumoto K, Nishiuchi T, Ahmed RA, Wong NC, Ueda K, Ishida T. Platelet derived growth factor regulates ABCA1 expression in vascular smooth muscle cells. *FEBS Lett.* 2006;580:4371–4376.

42. Zhuang L, Kim J, Adam RM, Solomon KR, Freeman MR. Cholesterol targeting alters lipid raft composition and cell survival in prostate cancer cells and xenografts. *J Clin Invest.* 2005;115:959–968.

43. Fielding CJ, Bist A, Fielding PE. Intracellular cholesterol transport in synchronized human skin fibroblasts. *Biochemistry.* 1999;38:2506–2513.

Ang II–stimulated migration of vascular smooth muscle cells is dependent on LR11 in mice

Meizi Jiang,[1] Hideaki Bujo,[1] Kenji Ohwaki,[2] Hiroyuki Unoki,[3]
Hiroyuki Yamazaki,[4] Tatsuro Kanaki,[2] Manabu Shibasaki,[2,4] Kazuhiko Azuma,[5]
Kenichi Harigaya,[5] Wolfgang J. Schneider,[6] and Yasushi Saito[2]

[1]Department of Genome Research and Clinical Application, [2]Department of Clinical Cell Biology, [3]Division of Applied Translational Research, and
[5]Department of Molecular and Tumor Pathology, Chiba University Graduate School of Medicine, Chiba, Japan. [4]Kowa Research Institute, Kowa Company Ltd.,
Higashimurayama, Japan. [6]Department of Medical Biochemistry, Max F. Perutz Laboratories, Medical University of Vienna, Vienna, Austria.

Medial-to-intimal migration of SMCs is critical to atherosclerotic plaque formation and remodeling of injured arteries. Considerable amounts of the shed soluble form of the LDL receptor relative LR11 (sLR11) produced by intimal SMCs enhance SMC migration in vitro via upregulation of urokinase-type plasminogen activator receptor (uPAR) expression. Here, we show that circulating sLR11 is a novel marker of carotid intima-media thickness (IMT) and that targeted disruption of the *LR11* gene greatly reduces intimal thickening of arteries through attenuation of Ang II–induced migration of SMCs. Serum concentrations of sLR11 were positively correlated with IMT in dyslipidemic subjects, and multivariable regression analysis suggested sLR11 levels as an index of IMT, independent of classical atherosclerosis risk factors. In *Lr11*$^{-/-}$ mice, femoral artery intimal thickness after cuff placement was decreased, and Ang II–stimulated migration and attachment of SMCs from these mice were largely abolished. In isolated murine SMCs, sLR11 caused membrane ruffle formation via activation of focal adhesion kinase/ERK/Rac1 accompanied by complex formation between uPAR and integrin $\alpha v\beta 3$, a process accelerated by Ang II. Overproduction of sLR11 decreased the sensitivity of Ang II–induced activation pathways to inhibition by an Ang II type 1 receptor blocker in mice. Thus, we demonstrate a requirement for sLR11 in Ang II–induced SMC migration and propose what we believe is a novel role for sLR11 as a biomarker of carotid IMT.

Introduction

Migration of vascular SMCs from the media to the intima is a key step in the development of atherosclerosis (1, 2). Following migration, SMCs proliferate in the intima and secrete matrices and proteases to form atheromatous plaques under the influence of stimulatory cytokines. The system encompassing urokinase-type plasminogen activator (uPA) and its receptor (uPAR) is thought to be important for the migration of SMCs. For migration, cell-associated proteolysis of ECM and/or receptor-mediated signaling leading to activation of ERK and Rac1 (3, 4) play crucial roles. However, in regard to migration of SMCs relevant to the development of atherosclerosis and remodeling of injured arteries, the mechanisms for and significance of uPA/uPAR activation have not been fully elucidated yet.

Functional studies using genetically altered animals or cells have revealed that certain receptors belonging to the family of LDL receptor relatives (LRs) are important regulators of cell migration via modulating cytokine signaling and/or protease activation (5–7). Interestingly, LR-mediated regulation of migration appears to be caused at least in part by modulation of the uPA/uPAR system (6,

7). LR11 (also called *sorLA*), an unusually complex and highly conserved LR discovered and molecularly characterized by us and others (8–10), mediates uPAR's plasma membrane localization, as both the membrane-spanning form and the shed soluble form of the receptor (sLR11) bind to and colocalize with uPAR on the cell surface (11). LR11 is highly expressed in intimal SMCs at the intima-media border in the plaque area of experimental models of atherogenesis (11, 12). Furthermore, overexpression of LR11 in SMCs enhances their migration via elevated levels of uPAR (13).

In the process of atherosclerosis, the BB isoform of PDGF (PDGF-BB) is an important cytokine for migration of SMCs (1, 2). PDGF-BB performs its task through the stimulation of cell motility via accelerated cytoskeleton rearrangement and degradation of ECM components of intimal SMCs (1). Also, PDGF-BB enhances migration of intimal SMCs via activation of the LR11/uPAR-mediated intracellular pathway (14). Ang II is another potent chemoattractant for SMCs (1, 15, 16). Recent studies with Ang II type 1 receptor (AT$_1$R) blockers (ARBs) (17) or knockdown experiments (18) have shown that intracellular signals involving activation of Rac1 are important for the Ang II–mediated hypertrophy of SMCs and neointimal formation in injured arteries.

Here, we have studied the (patho)physiological significance of the LR11-mediated migration system of intimal SMCs in the development of intimal thickening in vivo. We found that circulating sLR11 levels reflect the degree of carotid intima-media thickness (IMT), an established atherosclerosis marker (19), independently of other risk factors of IMT in subjects with dyslipidemia. Subsequent studies using LR11-targeted mice revealed that sLR11 increases membrane
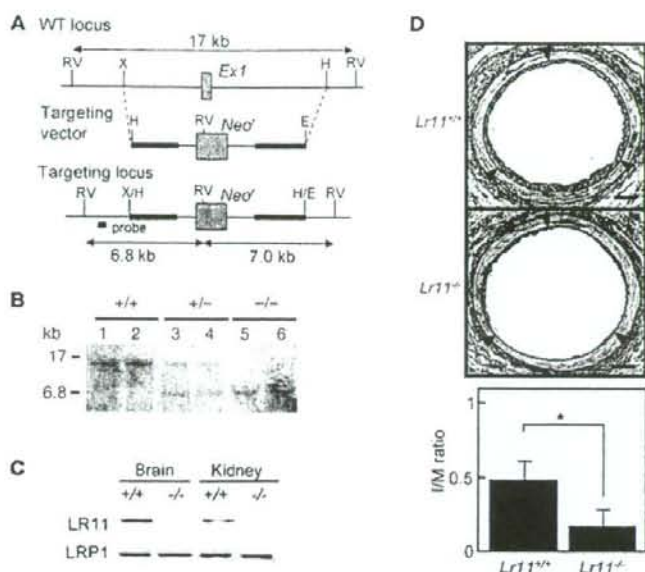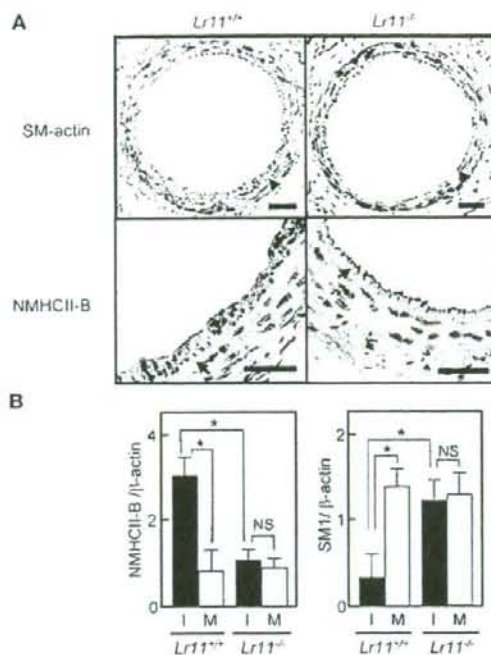
Figure 1
Intimal thickness of arteries after cuff placement in *Lr11⁻/⁻* mice. (**A**) Targeted disruption strategy of the murine *LR11* gene, consisting of 49 exons. The targeting vector (bold line) contains 3.3 kb (5′) and 4.4 kb (3′) of genomic DNA flanking the neomycin-resistance cassette (*Neoʳ*). After homologous recombination, *Neoʳ* replaced exon 1 (*Ex1*, gray box), which contained the initiation codon of the *LR11* gene. The location of the probe used for Southern blot analysis is shown. RV, *Eco*RV; X, *Xba*I; H, *Hind*III; E, *Eco*RI. (**B**) Southern blot analysis of murine-tail DNA from heterozygous intercrosses digested with *Eco*RV using the probe (see Figure 1A) that detects 17-kb and 6.8-kb fragments in the WT and knockout allele, respectively. (**C**) Immunodetection of LR11 protein. Total protein (100 μg) extracted from brain and kidney were separated by electrophoresis, blotted on a membrane, and incubated with antibody against LR11 (~250 kDa) or LRP1(~85 kDa). The samples were loaded on the same gel but not on immediately neighboring lanes. (**D**) Upper panels show sections of femoral artery of *Lr11⁺/⁺* or *Lr11⁻/⁻* mouse after cuff placement, subjected to elastica van Gieson staining. Arrowheads indicate the internal elastic layers. Scale bar: 50 μm. Lower panel shows I/M ratio of arteries presented as mean ± SD (*n* = 15). *P < 0.05.

studies using cultured SMCs (refs. 11–14, 20, and Supplemental Figure 1). We analyzed the effects of several other chemotactic cytokines (Ang II, VEGF, bFGF, and IL-6) on the migration activity of *Lr11⁻/⁻* SMCs (M. Jiang and H. Bujo, unpublished observations). Among them, only Ang II did not enhance the migration of *Lr11⁻/⁻* SMCs in both the presence and absence of PDGF-BB but did so in WT SMCs or *Lr11⁻/⁻* SMCs in the presence of conditioned medium from WT SMCs (Figure 3A). There were no significant differences in levels of Ang II–induced Stat1 phosphorylation activity between WT SMCs and *Lr11⁻/⁻* SMCs (Figure 3B). The absence of a migration response to Ang II of LR11-deficient SMCs prompted us to further analyze their motility properties, since Ang II is a potent stimulator of cytoskeleton reorganization through intracellular signaling (15, 17). Preincubation with Ang II of *Lr11⁺/⁺* SMCs but not of *Lr11⁻/⁻* SMCs enhanced cell attachment in the presence and absence of PDGF-BB (Figure 3C). The defect in the Ang II–mediated induction of attachment activity was restored by sLR11 in *Lr11⁻/⁻* SMCs (Figure 3D); note that the Ang II–induced attachment activity of *Lr11⁺/⁺* cells was reduced by neutralizing anti-LR11 antibodies to the levels observed in *Lr11⁻/⁻* SMCs. We therefore studied membrane ruffling, which is related to cytoskeletal reorganization leading to enhanced cell attachment (3, 4), in *Lr11⁺/⁺* and *Lr11⁻/⁻* SMCs. Ang II appeared to increase the proportion of cells with ruffles, and this increase was attenuated by blocking uPAR with neutralizing

antibody in *Lr11⁺/⁺* cells (Figure 4, A–C, D, and M). In *Lr11⁻/⁻* SMCs, Ang II's effect on ruffle formation was not significant; in addition, the proportion of cells with ruffles in the presence of PDGF-BB was lower (Figure 4, E–G, H, and M). Also, ruffling by Ang II incubation was not enhanced in *Lr11⁻/⁻* SMCs pretreated with sLR11 (Figure 4, I–M). Thus, as quantitated (Figure 4M), in the presence of PDGF, Ang II stimulates membrane ruffling of WT cells (Figure 4, B and C) and this stimulation is abolished in *Lr11⁻/⁻* SMCs (Figure 4, F and G), even in the presence of sLR11 (Figure 4, J and K). Surprisingly, sLR11 induces ruffle formation in *Lr11⁻/⁻* SMCs in the absence of both PDGF and Ang II (Figure 4, E and I), which is consistent with the sLR11-induced increase in attachment activity in *Lr11⁻/⁻* SMCs (see Figure 3D). The increased ruffling in the presence of sLR11 with PDGF and Ang II was almost abolished by blocking uPAR (Figure 4, K and L). Next, in order to study the significance of LR11 in the Ang II–mediated vascular pathology, we analyzed the effect of LR11 deficiency on intimal thickening of arteries after cuff placement in the murine Ang II infusion model. Administration of Ang II at 1 μg/kg/min for 28 days significantly increased the I/M ratio in *Lr11⁺/⁺* mice: note that the medial thickness in *Lr11⁺/⁺* mice was not significantly different from that in *Lr11⁻/⁻* mice (Figure 5A and Supplemental Figure 2). However, the Ang II infusion–induced increase was not observed in *Lr11⁻/⁻* mice. The increase by Ang II infusion in the level of NMHCII-B expression in intima versus

A

SM-actin

NMHCII-B

Lr11⁺/⁺   *Lr11⁻/⁻*

B

media did not occur in *Lr11⁻/⁻* mice (Figure 5B; note that the level of LRP1 after Ang II infusion remained unchanged in both *Lr11⁺/⁻* and *Lr11⁻/⁻* mice). Thus, *Lr11⁻/⁻* SMCs are characterized by a failure in Ang II–mediated ruffle formation and attachment, which in turn apparently leads to a decrease in Ang II– or PDGF-BB–mediated migration activity. Furthermore, Ang II infusion–induced intimal thickening in response to arterial injury is attenuated, accompanied by an altered expression pattern of myosin fiber isoforms in intimal SMCs (see Figure 2).

LR11 activates membrane ruffling through the uPAR/integrin/focal adhesion kinase/ERK/Rac1 pathway. LR11 binds to and colocalizes with uPAR on the cell surface (11), and a fraction of cell surface-located LR11 is proteolytically shed to produce a soluble form, sLR11 (22). To gain further insight into sLR11's activity, we analyzed its effect on uPAR-mediated intracellular signals for cytoskeletal reorganization. The proportion of cells with ruffle formation was increased in dose-dependent fashion by sLR11, and this increase was clearly reduced by pretreatment with neutralizing antibodies against LR11, uPAR, or integrin αvβ3; PD98059, a specific MEK inhibitor, had the same effect (Figure 6A). The formation of a complex between LR11 and integrin αvβ3 was shown by coimmunoprecipitation, as previously demonstrated for uPAR/LR11 (11). The complex formation was inhibited by the addition of known ligands of LR11, e.g., apoE and receptor-associated protein (RAP) (Figure 6B). LR11 attenuates internalization and catabolism of uPAR, which is accelerated by LRP1 (13). RAP, a common ligand of LR11 and LRP1, reduced the membrane expression of uPAR in *Lr11⁺/⁺* SMCs but significantly increased the uPAR expression in *Lr11⁻/⁻* SMCs (Figure 6C). Thus, LR11 in association with LRP1 appears to form a complex with integrin αvβ3 via interaction with uPAR, which also binds integrin (4, 11). Accordingly, sLR11 induced the phosphorylation

of focal adhesion kinase (FAK) and ERK, which act downstream of uPAR/integrin signals (Figure 7, A and B), and subsequent activation of Rac1 was detected in the presence of sLR11 (Figure 7C). Moreover, the activation of the FAK/ERK/Rac1 cascade was inhibited by neutralizing anti-integrin αvβ3 antibody (Figure 7, A–C). Likewise, in *Lr11⁻/⁻* cells, Rac1 activation was increased by sLR11, and this increase was diminished by neutralizing anti-integrin αvβ3 antibody (Figure 7D). In these experiments, the presence of anti-glutathione-S-transferase (anti-GST) antibody did not show any significant effects (data not shown). Thus, sLR11 can activate the FAK/ERK/Rac1 pathway in SMCs through complex formation with uPAR and integrin αvβ3; transduction of the signal leads to cytoskeletal reorganization associated with membrane ruffling.

Ang II induces migration of SMCs through activation of LR11-mediated cell attachment. Together with the results shown in Figures 6 and 7, the greatly diminished Ang II–induced migration in LR11-deficient SMCs (see Figure 3) suggested that it is due to a defect in Ang II's actions on the LR11/uPAR/integrin/FAK/ERK/Rac1 pathway. Ang II and PDGF-BB but not VEGF led to increased production of sLR11 in rabbit SMCs (Figure 8A). In fact, the levels of both sLR11 and membrane-bound LR11 but not LRP1 were increased by Ang II in a dose-dependent manner (Figure 8B). The Ang II–mediated increase in sLR11 levels was blocked by the ARBs, valsartan and candesartan, as well as by PD98059 (Figure 8C and Supplemental Figure 3). Ang II induced the membrane expression of uPAR in *Lr11⁺/⁺* SMCs, which was abolished in *Lr11⁻/⁻* SMCs (Figure 9A). Thus, the specific increase of sLR11 levels caused by Ang II together with the reduction in Ang II–induced migration and attachment in *Lr11⁻/⁻* SMCs (see Figure 3) strongly suggested that Ang II is key to enhanced migration via activation of the LR11-mediated pathway and cytoskeletal reorganization. Accordingly, Ang II–induced Rac1 activation was inhibited by neutralizing antibody against LR11 or uPAR (Figure 9B). The abolished Ang II–induced Rac1 activation in *Lr11⁻/⁻* SMCs was recovered by sLR11, and the sLR11-mediated activity was not inhibited by candesartan (Figure 9C). The Ang II–induced increase in cell attachment was abolished by a neutralizing antibody against LR11, and importantly, valsartan had no effect on Ang II–induced enhanced attachment in the presence of sLR11 (Figure 10A). In addition, Ang II–induced migration activity was suppressed when SMCs were pretreated with uPAR-specific siRNA (Figure 10B). Finally, the inhibitory abilities of valsartan and candesartan on migration activity were reduced in sLR11-pretreated C-1 cells (16% and 17%, respectively), an established SMC line (11), or LR11-overexpressing R-1 cells (20% and 11%, respectively) compared with untreated C-1 cells (34% and 35%, respectively), although the absolute extent of inhibition among them were similar (Figure 10C). These results indicate that Ang II

— 204 —
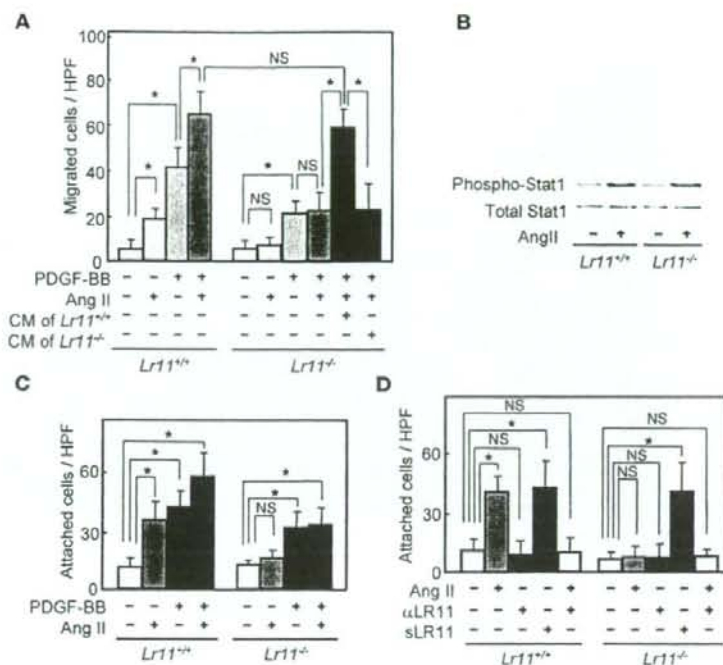
Figure 3
Ang II–induced migration and attachment of cultured SMCs derived from $Lr11^{-/-}$ mice. (A) Effect of Ang II on the PDGF-BB–induced (10 ng/ml) migration activities of $Lr11^{+/+}$ or $Lr11^{-/-}$ SMCs. SMCs were incubated with 1 μM Ang II for 24 hours in the presence or absence of conditioned medium of $Lr11^{-/-}$ SMCs before migration analyses. Data are presented as mean ± SD ($n = 6$). (B) Effect of Ang II on Stat1 phosphorylation in $Lr11^{+/+}$ or $Lr11^{-/-}$ SMCs. SMCs were incubated with 1 μM Ang II for 10 minutes before immunoblot analysis for (phospho-) Stat1 (~90 kDa). (C) Effects of Ang II on cell attachment of $Lr11^{+/+}$ or $Lr11^{-/-}$ SMCs in the presence or absence of 10 ng/ml PDGF-BBs. SMCs were incubated with or without Ang II (1 μM) for 24 hours before attachment analyses. Data are presented as mean ± SD ($n = 6$). (D) Effects of sLR11 on Ang II–induced attachment of $Lr11^{+/+}$ or $Lr11^{-/-}$ SMCs. SMCs were incubated with or without Ang II (1 μM) for 24 hours in the presence or absence of anti-LR11 antibody (pm11, 1:5 dilution) or recombinant sLR11 (1 μg/ml) for 24 hours before attachment analyses. Data are presented as mean ± SD ($n = 6$). *$P < 0.05$.

induces cell migration through activation of LR11/uPAR-mediated cell attachment involving the Rac1 pathway.

Candesartan does not inhibit intimal thickening after arterial injury in mice overproducing sLR11. The production of sLR11 is elevated in SMCs in the course of intimal thickening after endothelial injury (20). In order to learn more about the effects of inhibition of Ang II–mediated LR11/uPAR/integrin signaling on intimal thickening, we analyzed the intimal thickness after cuff placement in LR11-overexpressing mice. Mice were implanted with R-1 cells, which are A7r5 cells stably overexpressing LR11, or with mock-transfected A7r5 cells (C-1) (13, 23). Mice implanted with R-1 cells showed a 5.2-fold increase in the serum concentration of immunodetectable sLR11 after implantation compared with those implanted with C-1 cells (4.2 ± 2.6 U versus 0.8 ± 0.1 U). Candesartan administration significantly reduced the intimal thickness (I/M ratio) 4 weeks after cuff placement in C-1 but not in R-1 mice (note that treatment of R-1 mice with neutralizing antibody against uPAR reduced the intimal thickness; Figure 11, A–J and U). Intimal versus medial expression of LR11 and NMIICII-B was significantly reduced by candesartan in C-1 mice (Figure 11, K, L, P, Q, and V). In contrast, the levels of LR11 and NMIICII-B expression in intima versus media were not signifi-

cantly different in R-1 mice whether treated with candesartan or not (note that treatment of R-1 mice with neutralizing antibody against uPAR did not significantly reduce the ratio of intimal to medial expression of LR11; Figure 11, M–O, R–T, and V). Thus, the ARB candesartan, which inhibits Ang II–mediated LR11/uPAR/integrin cell migration and attachment signals, reduces intimal thickness after cuff placement in mice; this reduction is counteracted in mice that overproduce sLR11. These results, obtained using an intimal thickening model with sLR11 overproduction, show that Ang II–induced cell migration and attachment contribute to the migration of SMCs from the media to the intima after arterial injury.

Discussion

LRs play a key role in the catabolism of complexes between proteinases and their receptors (5–7). In SMCs, LRs are thought to function in the catabolism of membrane molecules that regulate intracellular signaling events important for the specific properties of these cells, particularly in regard to their motility and migration (24–33). Members of the family, such as LRP1 (34), VLDL receptor (LR8) (25), and LRP1B (32, 35), endocytose uPAR and uPA/uPAR complexes into cells for subsequent degradation
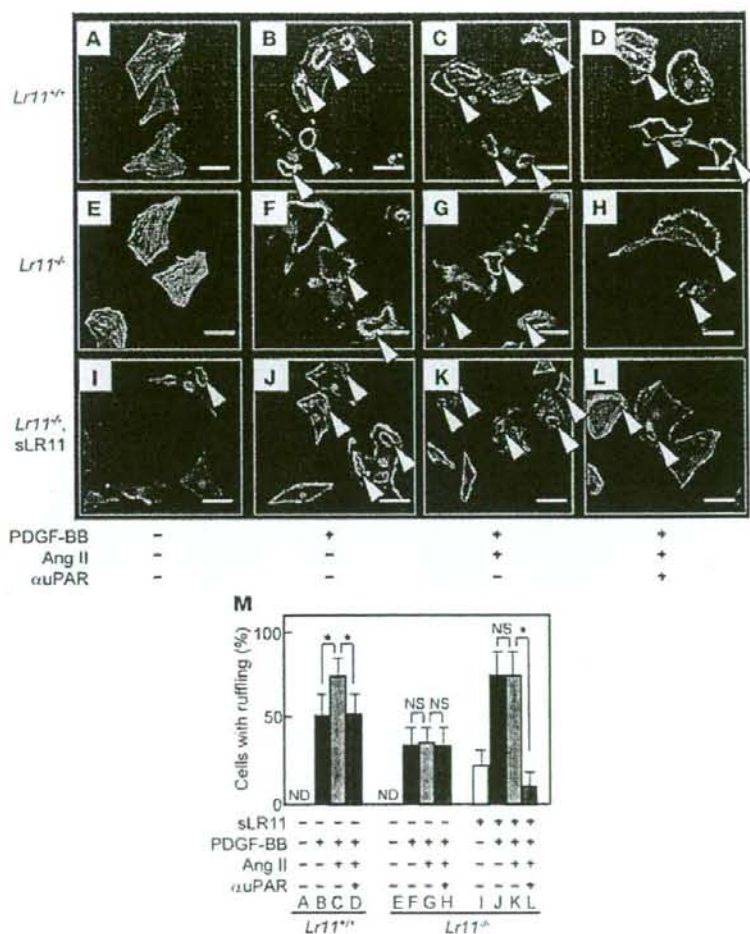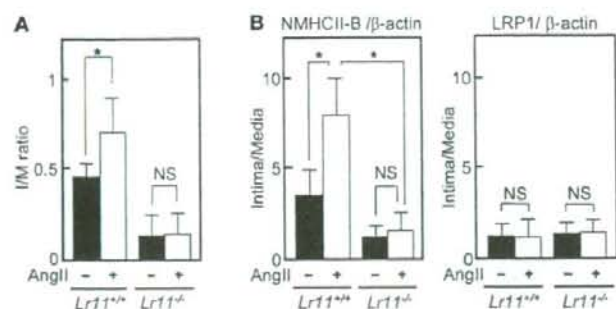
Figure 4
Ang II–induced membrane ruffle formation of cultured SMCs derived from *Lr11⁻/⁻* mice. (A–L) Ang II–induced membrane ruffling (arrowheads) in *Lr11⁺/⁺* or *Lr11⁻/⁻* SMCs. The indicated SMCs were incubated with or without Ang II (1 μM) for 24 hours in the presence or absence of recombinant sLR11 (1 μg/ml) with or without anti-uPAR antibody for 24 hours. PDGF-BB (10 ng/ml) was then added to the culture medium for 10 minutes before immunofluorescence analyses. Cells were then stained using Alexa Fluor 488 phalloidin. Scale bars: 10 μm. (M) The number of cells with membrane ruffles were counted among 500 cells in the field. Data are presented as mean ± SD (*n* = 3). *P < 0.05. ND, not detected.

and/or recycling. We have discovered what we believe is a novel mechanism for uPAR localization to the plasma membrane that involves LR11 (11). Recycling and degradation of uPAR on the membrane is dependent on its internalization via LRP1 (34). The extracellular sLR11 binds to and colocalizes with uPAR on the cell surface; this de facto immobilization effectively stabilizes the receptor-protease complex by inhibiting its degradation through LRP1 (11). In cultured SMCs, LR11 is highly expressed, but LRP1 expression is rather stable during the rapidly proliferating phase (32). The balance between expression levels of LR11 and LRP1 may be important for the regulation of uPAR expression in the membrane (see Figure 6C). Enhanced uPAR-mediated cell migration appears to constitute an important factor in the process of ath-

erosclerosis and arterial modeling (3, 4). LR11 is highly expressed in atherosclerotic plaques, particularly in the intimal SMCs at the border between the intima and the media in plaques of humans and apoE-knockout mice (11, 32). Considerable amounts of sLR11 are produced by intimal SMCs in the process of intimal thickening after cuff injury of femoral arteries in mice (20). In this study, an attempt to investigate the clinical significance of circulating sLR11 levels in atherosclerosis was made in relation to dyslipidemia, since LR11 is a relative of the LDL receptor, a key receptor for maintenance of lipid homeostasis (1, 5–7). We discovered that circulating sLR11 levels are positively correlated with the degree of carotid IMT, representative of arterial intimal and medial thickness and closely associated with the development of coronary and/or cere-

Figure 5
Intimal thickening after cuff placement in response to Ang II infusion in Lr11−/− mice. (**A**) I/M ratios of femoral arteries in Lr11+/+ or Lr11−/− mice after cuff placement with saline or Ang II infusion (1 μg/kg/min for 28 days) are presented as mean ± SD (n = 15). *P < 0.05. (**B**) mRNA levels of NMHCII-B and LRP1 in injured arteries. Total RNA isolated from the intima or the media of Lr11+/+ or Lr11−/− mice was reverse transcribed into cDNA and subjected to real-time PCR analysis using specific primers for NMHCII-B and LRP1, respectively. The amounts of amplified products are expressed relative to the amounts of β-actin transcript, and the ratio of mRNA expression levels of intima and media are presented as mean ± SD (n = 3). *P < 0.05.

bral artery diseases (19). and that this correlation is independent of other established risk factors for IMT in subjects with dyslipidemia. Taking the results together, we propose that circulating sLR11 may be a marker reflecting the intimal and medial thickness of injured arteries. Clearly, further careful studies using subjects with different characteristics are needed for the evaluation of a (patho)physiological significance in arterial diseases. Given that sLR11 is released from other major sources, the basis for this inference remains uncertain. Considering that (a) the changes in IMT are presumably due to the evaluation of the complex of intimal thickness, medial thickness, and hypertrophy of SMCs, which can result from hypertension in the carotid arteries, and (b) LR11 is required for Ang II–induced SMC migration in culture systems and mouse models, the relation of the current results to the pathology of hypertension-induced vessel damage requires attention. sLR11 may well affect the remodeling of injured arteries through the phenotypic conversion of medial SMCs, since loss of sLR11 disturbs the myosin isoform conversion in addition to the actin rearrangement in SMCs (see Figure 2B, Figure 5B, and Supplemental

Figure 1A). In this context, the pathophysiological alteration of Lr11−/− SMCs in the medial layer after Ang II infusion needs to be evaluated by a model suitable for vessel remodeling in addition to the current cuff placement model (see Figure 5A). In any case, the major sources and the plasma concentrations of sLR11 in various conditions need to be identified. In the process of atherosclerosis and vascular restenosis after coronary angioplasty, the migration of SMCs appears to play a key role in intimal thickening (1, 2). SMCs acquire or lose numerous cellular functions required for performing the above tasks in the intima, as represented by changes in myosin isoforms including NMHCII-B and SM1 (14, 21). One of these tasks is enhancing cellular mobility while interacting with components of the basement membrane and other extracellular matrix components. One of the players in matrix degradation is uPA bound to its specific receptor, uPAR, on the cell surface; its essential role in enhancing cell mobility has been intensively studied in cancer invasion and neural migration (3, 4). uPAR interacts with integrin αvβ3 (36) and subsequently activates signaling pathways such as the FAK/ERK/Rac1 cascade for cytoskeleton reor-
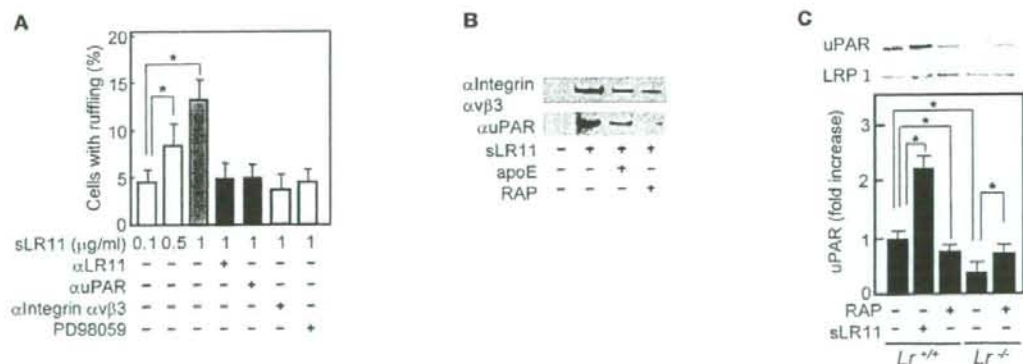
Figure 6
sLR11-mediated ruffle formation through complex formation with uPAR and integrin αvβ3. (**A**) sLR11-induced membrane ruffle formation. Rabbit SMCs were incubated with sLR11 (1 μg/ml) for 24 hours in the presence or absence of antibody against LR11, uPAR, or integrin αvβ3 (MAB1976) or of PD98059. The number of cells with membrane ruffles were counted among 500 cells in the field. Data are presented as mean ± SD (n = 5). (**B**) Coimmunoprecipitation of sLR11 (~250 kDa) with integrin αvβ3 or uPAR. Membrane extracts of rabbit SMCs were incubated with or without sLR11 in the presence or absence of apoE (50 μg/ml) or RAP (10 μg/ml), immunoprecipitated with anti-integrin αvβ3 or anti-uPAR antibody, and subjected to immunoblot analysis using anti-LR11 antibody. (**C**) uPAR expression in Lr11−/− SMCs. Membrane extracts of Lr11+/+ or Lr11−/− SMCs were incubated with RAP and subjected to immunoblot analysis using anti-uPAR (~50 kDa) or anti-LRP1 (~85 kDa) antibody. Blot shown is representative of 3 independent experiments. Data are presented as mean ± SD (n = 3). *P < 0.05.
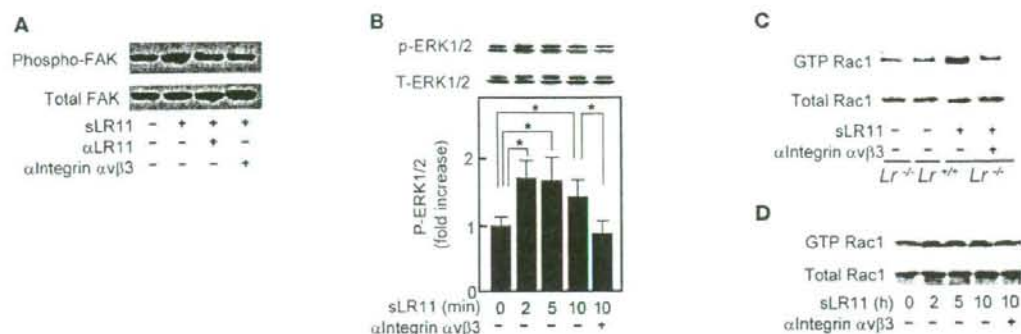
Figure 7
sLR11-mediated intracellular signals related to cytoskeleton reorganization. (**A**) sLR11-induced FAK activation. Cell lysates of rabbit SMCs were incubated with or without sLR11 (1 μg/ml) in the presence or absence of antibody against LR11 or integrin αvβ3 (MAB1976), immunoprecipitated with anti-FAK antibody, and subjected to immunoblot analysis using anti-FAK (–130 kDa) or anti–phospho-FAK (–130 kDa) antibody. (**B**) sLR11–induced phosphorylation of ERK1/2. Cell lysates (10 μg protein) of rabbit SMCs were incubated with sLR11 (1 μg/ml) for the indicated times in the presence or absence of anti–integrin αvβ3 antibody (MAB1976) and subjected to immunoblot analysis using antibody against (phospho) p42/44 MAP kinase. Upper and lower signals represent ERK1 (–44 kDa) and ERK2 (–42 kDa), respectively (13). Blot shown is representative of 3 independent experiments. Data of p-ERK1/2 are presented as mean ± SD (n = 3). *P < 0.05. (**C**) Rac1 activation in $Lr11^{-/-}$ SMCs. Cell lysates (60 μg protein) of $Lr11^{+/+}$ or $Lr11^{-/-}$ SMCs were incubated with sLR11 (1 μg/ml) in the presence or absence of antibody against integrin αvβ3 (RMV-7), immunoprecipitated with PAK-1 PBD Protein GST beads, and subjected to immunoblot analysis with anti–Rac1 (–21 kDa) or anti–GTP-Rac1 (–21 kDa) antibody. (**D**) sLR11-induced Rac1 activation. Cell lysates (60 μg protein) of rabbit SMCs were incubated with sLR11 (1 μg/ml) for the indicated times in the presence or absence of anti–integrin αvβ3 antibody (MAB1976) and subjected to immunoblot analysis with anti-Rac1 (Rac1 –21 kDa and GST-Rac1 –21 kDa) antibody with (top) or without (bottom) prior immunoprecipitation with PAK-1 PBD Protein GST beads.

ganization (3, 4). Therefore, uPAR activation contributes to the progression of vascular remodeling through enhanced migration of intimal SMCs. Based on these findings, we have now identified a regulator of uPAR-mediated activation of cytoskeletal reorganization in the process of Ang II–induced migration of SMCs (see Figure 12). Moreover, the disturbed myosin isoform conversion in $Lr11^{-/-}$ SMCs may indicate that the LR11/uPAR signal plays a role in the coordination of actin and myosin rearrangement. The significance of LR11-mediated cytoskeleton reorganization for the conversion from contractile to synthetic phenotype needs to be addressed in future studies.

Ang II, similar to PDGF-BB, plays an important role as a cytokine in the process of atherosclerosis and vascular remodeling (15, 16). The activation of its specific receptor, AT_1R, triggers various intracellular signals toward proliferation and migration of SMCs. The Ang II-promoted activities are greatly diminished by specific AT_1R antagonists or by inhibition of MAP signaling using synthetic inhibitors of MAP kinase (3, 4). Here, Ang II stimulated cell migration and attachment and LR11 expression through AT_1R activation; the enhancement of attachment by Ang II was more obvious in the absence than in the presence of PDGF-BB (see Figure 3). Blocking LR11 and subsequent events abolished Ang II–induced migration and attachment of SMCs (see Figure 10). The effects of LR11 ablation on Ang II–induced migration and attachment strongly suggest that Ang II–mediated enhancement of attachment depends on sLR11-mediated cytoskeleton reorganization. sLR11-induced ruffle formation and attachment activity even in the absence of Ang II or PDGF-BB (see Figure 3D, Figure 4, I and M, and Figure 10C) suggest that LR11 overproduction generally induced by such cytokines is important for the increased attachment activity through enhanced ruffle formation in the process of cell migration.

ARBs prevent vascular damages in a mouse model of Marfan syndrome through amelioration of the increased activation of TGF-β signaling pathways (37). Boucher et al. recently reported on a conditional LRP1-deficient mouse model in which activation of TGF-β signaling pathways in the vascular wall was maximally increased, which is similar to what occurs in Marfan syndrome (38). LR11 seems to play an essential role in the change in cell mobility in the signals from Ang II and also in part from PDGF-BB (Figure 12).

Neutralizing antibodies against LR11 have been shown to reduce the migratory activity of intimal SMCs and intimal thickness after cuff injury (11). Here, using LR11-deficient cells, we found that sLR11 induces the complex formation of uPAR and integrin αvβ3 in SMCs (Figure 6). This finding may well explain the previous observation that incubation with aprotinin, a plasmin inhibitor, effectively reduces invasion but has much less effect on migration in LR11-overexpressing cells (ref. 13 and Supplemental Figure 1). The current study shows that overproduction of sLR11 in the absence of the membrane-bound form triggers the activation of uPAR-mediated intracellular signals via the integrin/ ERK/Rac1 pathway, leading to membrane ruffling (Figures 6 and 7). Elevated sLR11 levels resulted in an exaggerated response of intimal SMCs to vascular injury and to an attenuated sensitivity to ARB treatment in mice (Figure 11). In this context, we recently observed that exogenous recombinant sLR11 interacts with macrophage uPAR and accelerates foam cell formation (20). Thus, sLR11 derived from intimal SMCs is implicated in plaque formation through its effects on SMCs and macrophages. Although our limited analysis did not show a significant relationship between sLR11 and high-sensitive C-reactive protein (hsCRP) in plasma (M. Jiang and H. Bujo, unpublished observations), the involvement of inflammation in LR11 gene expression or shedding of sLR11 in
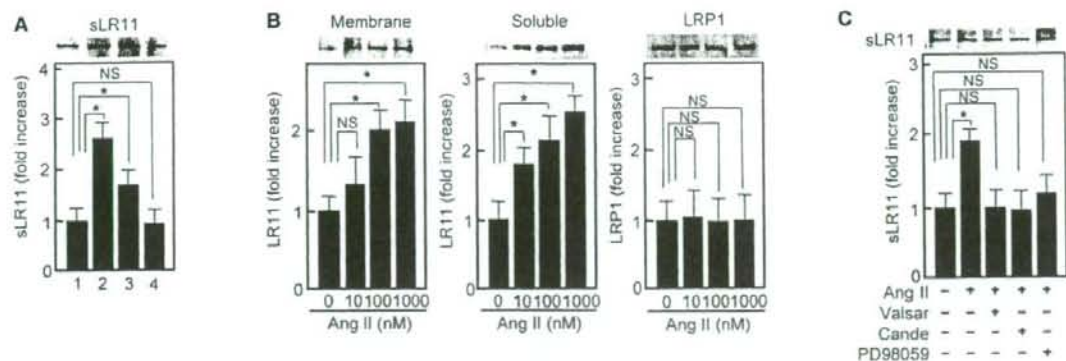
Figure 8
Ang II–induced sLR11 production in SMCs. (**A**) Effects of chemotactic cytokines on the production of sLR11 in rabbit SMCs. Conditioned media collected for 12 hours in the absence (lane 1) or presence of Ang II (1 μM, lane 2), PDGF (10 ng/ml, lane 3), or VEGF (50 ng/ml, lane 4) were concentrated and subjected to immunoblot analysis using anti-LR11 antibody (~250 kDa). Blot shown is representative of 3 independent experiments. Data are presented as mean ± SD ($n = 3$). *$P < 0.05$. (**B**) Ang II–dependent increase of soluble or membrane-bound forms of LR11 in SMCs. Membrane extracts (20 μg protein) prepared from rabbit SMCs or conditioned medium collected for 12 hours after the addition of Ang II at the indicated concentrations were subjected to immunoblot analysis with anti-LR11 (~250 kDa) or anti-LRP1 (~85 kDa) antibody. Blot shown is representative of 3 independent experiments. Data are presented as mean ± SD ($n = 3$). (**C**) Effect of ARBs or an ERK inhibitor on the Ang II–dependent increase in sLR11 in rabbit SMCs. Conditioned medium collected for 12 hours in the presence or absence of Ang II with or without valsartan (valsar, 10 nM), candesartan (10 nM), or PD98059 (10 μM) were subjected to immunoblot analysis with anti-LR11 (~250 kDa) antibody. Blot shown is representative of 3 independent experiments. Data are presented as mean ± SD ($n = 3$).

various diseases accompanied with vascular damage needs to be evaluated in future studies.

It is of interest that in the central nervous system, LR11 directs trafficking of amyloid precursor protein into recycling pathways (39) and LR11 expression is reduced in sporadic Alzheimer disease (40). We have recently shown that inherited *LR11/SORL1* variants are associated with late-onset Alzheimer disease (39). Furthermore, soluble circulating LRP1 has been shown to provide key endogenous peripheral "sink" activity for amyloid β-peptide in humans (41). The functions of LR11 in amyloid precursor protein and uPAR catabolism in association with LRP1 suggest multiple roles for LR11 in the degradation and/or transport of several cell-surface and cytoplasmic molecules. In any case, the vascular phenotype of LR11 deficiency, i.e., severely disturbed Ang II–mediated migration of SMCs through decreased uPAR catabolism, provides a system for studies on the regulation of vascular remodeling toward the development of novel therapeutic interventions.

Methods

Subjects. The study subjects are participants in a cohort study carried out concurrently with health-check screening at Awa area in Chiba, Japan (42). From among the 22,228 participants screened initially, we selected individuals with dyslipidemia (LDL cholesterol [LDL-C] > 160 mg/dl, triglycerides > 200 mg/dl, or HDL-cholesterol [HDL-C] < 35 mg/dl). None of the selected participants had medical complications or was undergoing treatment for abnormal plasma lipids, glucose, or blood pressure levels. The selected participants visited a hospital for detailed examination of their clinical profiles, collection of fasting blood samples, and measurement of carotid IMT. None had diabetes mellitus or thyroid and endocrinological diseases. All gave written informed con-

sent prior to the study, which was approved by the Human Investigation Review Committee of the Chiba University Graduate School of Medicine. Examination of IMT was carried out with an ultrasound scanner (SSD-1200CV; ALOKA) equipped with a linear 7.5-MHz transducer (32, 43). IMT was defined as the distance from the leading edge of the lumen-intima interface to the leading edge of the media-adventitia interface of the far wall. The measurement of IMT in the common carotid artery was made along a 10-mm section just proximal to the carotid bulb (32, 43), and the average IMT was calculated from the right and left IMTs of common carotid arteries. Venous blood was drawn after an overnight fast of 12–14 hours. Serum was separated from blood cells by centrifugation and used for the measurement of lipids and other biochemical markers (2). LDL-C was estimated with the equation of Friedewald (32). LDL particle size and malondialdehyde-LDL levels were determined using gradient gel electrophoresis and sandwich ELISA, respectively (32). sLR11 was immunologically measured as described in Immunoblotting and immunoprecipitation.

Generation of Lr11⁻⁻ mice. A plasmid-targeting vector was constructed with 3.3 kb (5′) and 4.4 kb (3′) of genomic DNA flanking the neomycin resistance cassette (*Neoʳ*) to target the first exon of murine LR11. After linearization, the plasmid was introduced into 129/Sv-derived embryonic stem cells by electroporation. Homologous recombinants were identified, and 2 independently targeted clones were injected into C57BL/6 blastocysts to generate chimeric mice. Male chimeras were crossbred with C57BL/6 females, and germline transmission was verified by Southern blot analysis. For Southern blot analysis, genomic DNA was prepared from the tail and digested with *EcoRV*. The fragments were separated by electrophoresis, transferred to a membrane, and hybridized with specific fragments corresponding to flanking regions of homologous recombination as probes for the identification of *Lr11⁺⁺*, *Lr11⁺⁻*, and *Lr11⁻⁻* mice, as described previously (44). All animal studies were
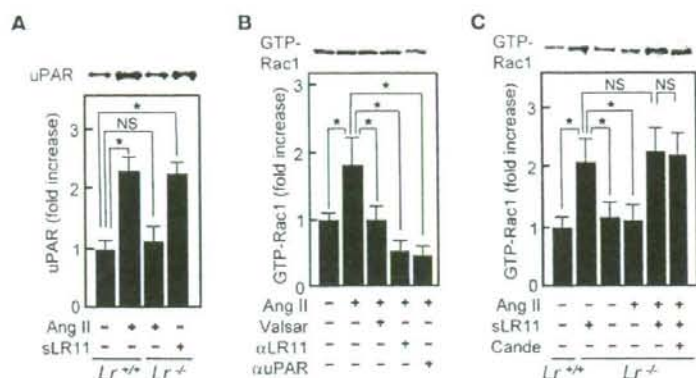
Figure 9
Ang II–induced LR11/uPAR pathway in SMCs. (A) uPAR expression in *Lr11⁻ᐟ⁻* SMCs. Membrane extracts of *Lr11⁺ᐟ⁺* SMCs or *Lr11⁻ᐟ⁻* SMCs were incubated with or without Ang II (1 μM) in the presence or absence of sLR11 (1 μg/μl) and subjected to immunoblot analysis using anti-uPAR (~50 kDa) antibody. Blot shown is representative of 3 independent experiments. Data are presented as mean ± SD (*n* = 3). *P < 0.05. (B) Effect of blocking the LR11/uPAR pathway on the Ang II–dependent increase of Rac1 activation in rabbit SMCs. Cell lysates (60 μg protein) were incubated in the presence or absence of Ang II (1 μM) with or without valsartan (10 nM), anti-LR11 antibody, or anti-uPAR antibody, immunoprecipitated with PAK-1 PBD Protein GST beads, and subjected to immunoblot analysis using anti-Rac1 (~21 kDa) antibody. Blot shown is representative of 3 independent experiments. Data are presented as mean ± SD (*n* = 3). (C) Effect of ARB on the Ang II–dependent increase of Rac1 activation in *Lr11⁻ᐟ⁻* SMCs. Cell lysate (60 μg protein) of *Lr11⁺ᐟ⁺* or *Lr11⁻ᐟ⁻* SMCs was incubated in the presence or absence of Ang II (1 μM) with or without candesartan (10 nM) or sLR11 (1 μg/μl), immunoprecipitated with PAK-1 PBD Protein GST beads, and subjected to immunoblot analysis using anti-Rac1 (~21 kDa) antibody. Blot shown is representative of 3 independent experiments. Data are presented as mean ± SD (*n* = 3).

approved by the Special Committee on Animal Welfare, School of Medicine, at the Inohana Campus of Chiba University.

Vascular injury by cuff placement. Cuff-placement surgery was carried out on 20-week-old male mice, as described (11). After isolating the right femoral artery from the surrounding tissues, a polyethylene tube (2-mm PE-90; BD) was opened longitudinally, loosely placed around the artery, and then closed with sutures. These arteries were removed from mice after 4 weeks; this was followed by serial perfusion with PBS(-) and with 10% neutral buffered formalin at 100 mmHg. The tissue was fixed in 10% neutral buffered formalin overnight, dehydrated, and embedded in paraffin. The middle segment of the artery was cut into subserial 5-μm cross sections with an interval of 50 μm between them. The sections were stained with elastica van Gieson or used for subsequent histochemical analyses. The image analysis software WinROOF (Mitani Corp.) was used to measure the areas of the intima and the media, respectively.

Laser capture microdissection. Frozen samples of cuffed artery were immediately embedded in OCT medium (Tissue-Tek; QIAGEN) and allowed to equilibrate to the cryostat temperature of -20°C. Each sample was sectioned into 10-μm specimens, placed on slides (Arturus; Molecular Devices), and directly fixed in fresh 95% ethanol. After complete dehydration, the slides were placed in solutions of 75% ethanol for 30 seconds, 95% ethanol for 30 seconds, 100% ethanol for 30 seconds, and xylene for 5 minutes, then allowed to dry. SMCs in intimal and medial layers were captured for subsequent RNA experiments using a PixCell II Laser Capture Microdissection System (Molecular Devices).

Ang II infusion. The surgical procedures for connection to ALZET osmotic minipumps were performed together with those for cuff placement in *Lr11⁺ᐟ⁺* and *Lr11⁻ᐟ⁻* mice. The pumps delivered either saline or Ang II at a rate of 1 μg/kg per minute. The arteries were removed from mice after 4 weeks.

Antibodies, recombinant proteins, and ARBs. Mouse monoclonal (5-4-30-19-2) and rabbit polyclonal (pm11) antibodies against LR11 were described

previously (11). Polyclonal antibodies against uPAR (AF807), NMHCII-B (PRB-445P), integrin αV (RMV-7), GST (A-30), and (phospho-) p44/42 MAP kinase and (phospho-) Stat1 were from R&D Systems, Covance, BioLegend, BostonBiochem, and Cell Signaling Technology, respectively. Monoclonal antibodies against LRP1, SMA (1A4), FAK (MAb2A7), p-Y397 of FAK, and integrin αvβ3 (MAB1976) were from Research Diagnostics Inc., Dako, Upstate Biotechnology (Millipore), BioSource (Invitrogen), and Chemicon (Millipore), respectively. Recombinant PDGF-BB, angiotensin II, VEGF, and plasmin were from R&D Systems, Sigma-Aldrich, Wako, and American Diagnostica, respectively. apoE and 39-kDa RAP were from Cosmo Bio Co. Ltd. Recombinant sLR11 protein lacking the 104 C-terminal amino acids containing the transmembrane region (sLR11) was prepared as described (20). Purified sLR11 was used for experiments at a concentration of 1 μg/ml, estimated from its biological activity in stimulating the migration of rabbit SMCs. The ARBs valsartan (CGP48933) and candesartan (CV-11974) were obtained from Novartis and Takeda Pharmaceutical Co. Ltd., respectively.

Cells. Primary cultures of mouse SMCs were prepared as described (45). In brief, the whole aortae prepared from 10-week-old mice were cut into pieces of approximately 1 mm² after removal of adventitial connective tissue and luminal endothelial cells. The pieces were digested with 1 mg/ml collagenase (Nitta Gelatin Inc.) and 20 U/ml elastase (Elastin Products Co. Inc.) in DMEM (Sigma-Aldrich) for 30 minutes at 37°C, and centrifuged at 2,000 g for 10 minutes at 4°C. The precipitate was resuspended in DMEM supplemented with 10% FBS (GIBCO; Invitrogen) and 40 μg/ml gentamycin (Schering-Plough). After 2 to 10 passages, cells from the primary culture were used for experiments. Primary cultures of rabbit SMCs were prepared from the medial layers of aortae as described (13) and used at passages 3 and 4. The LR11-overexpressing A7r5 cells (a rat embryonic aortic SMC line), R-1, and the control line C-1 were established as described (13). Before migration, biochemical, and immunological assays, cells were preincubated with various agents under the
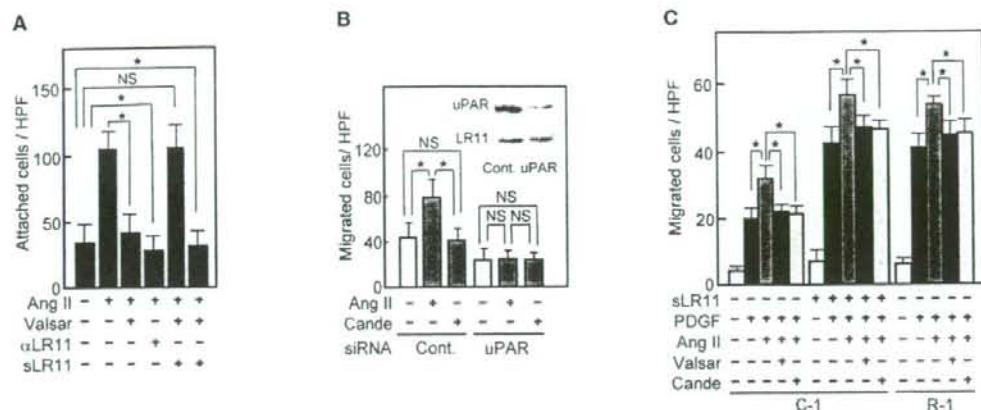
Figure 10
Ang II–induced migration via the LR11/uPAR pathway in SMCs. (**A**) Effect of blocking LR11 activation on the Ang II–induced increase of attachment of rabbit SMCs. The SMCs attached to plastic plates were counted after incubation in the presence or absence of Ang II (1 μM) with or without valsartan (10 nM), anti–LR11 antibody, or sLR11 (1 μg/μl). Data are presented as mean ± SD (n = 3). *P < 0.05. (**B**) Effect of uPAR silencing on the Ang II–induced increase in rabbit SMCs migration. The migrated SMCs treated with exogenous siRNA specific for uPAR or control (Cont.) RNA were counted after incubation in the presence or absence of Ang II (1 μM) with or without candesartan (10 nM). Inset: Membrane extracts (10 μg protein) prepared from these cells were subjected to immunoblot analysis with anti–uPAR (~50 kDa) or anti–LR11 antibody (~250 kDa). Data are presented as mean ± SD (n = 3). (**C**) Effect of Ang II on the PDGF–induced migration of LR11-overexpressing SMCs. The number of migrated A7r5 cells transfected with LR11 cDNA (R-1), or control cells (C-1) in the presence or absence of PDGF-BB (PDGF, 10 ng/ml) were determined after incubation with or without sLR11 (1 μg/μl), Ang II (1 μM), or valsartan (10 nM). Data are presented as mean ± SD (n = 10).

conditions indicated in the figure legends at 37°C, and then aliquots of the cell suspension were used for the experiments.

RT-PCR. Total RNA was purified from the microdissected or cultured cells using an RNeasy kit (QIAGEN) as described (11). The methods for RT-PCR have been described (46). The amplified products were visualized after gel electrophoresis. For quantification of transcript levels, real-time PCR was performed using SYBR Green PCR master mix (Applied Biosystems). The sequences of the PCR primers were according to known cDNA sequences: LR11, 5'-AATGGTGTTTGGTTGAAACACACATCT-TAG-3' and 5'-TACGTGGTTTCAACTACCAGAAATGCGCTT-3'; LRP1, 5'-CGGAACTGTACCATTTCA-3' and 5'-GGTGTTGACAACCCATTCG-3'; NMMHCII-B, 5'-TGGAGGATCCCGAGAGGTATCT-3' and 5'-GGAATCCACACCAGCTTTTTAGC-3'; SM1, 5'-CTCAAGAGCAAACT-CAGGAG-3' and 5'-TCTGTGACTTGAGAACGAAT-3'; β-actin, 5'-AGAGGGAAATCGTGCGTGAC-3' and 5'-CAATAGTGATGACCTG-GCCGT-3'. mRNA amounts were normalized to levels of β-actin mRNA, which served as the internal standard.

Migration, invasion, attachment, and proliferation assays. Cell migration and invasion were measured essentially as previously described (13), using a 96-well micro-Boyden chamber, its surface coated with type I collagen, and Transwell (Corning) 24-well plates coated with 100 μl collagen gel, respectively. The lower chamber contained 1% FBS-DMEM with or without 10 ng/ml PDGF-BB. After a 4-hour incubation at 37°C, the cells on the upper surfaces were washed, fixed, and stained by Diff-Quik (International Reagents Corp.). The number of cells that migrated to the lower (outer) surface of the filters (high-power field) was determined microscopically by counting. Cell adhesion was determined in a 96-well plate, the surface of which was coated with type I collagen, as described (20). After a 2-hour incubation at 37°C, nonadherent cells were removed by gently washing with PBS and adherent cells were determined by counting. Cell proliferation was measured based on the incorporation of BrdU during DNA synthesis of proliferating cells

using a cell proliferation ELISA system (Amersham). In brief, after 48-hour incubation at 37°C without FBS, SMCs (8,000 cells/well) were labeled with BrdU (10 μmol/l) in the presence or absence of Ang II for 8 hours. DNA synthesis was assessed by measuring the amount of BrdU incorporation into the DNA, which was detected by the above immunoassay system.

Immunoblotting and immunoprecipitation. Cultured cells were washed 3 times with PBS and harvested in PBS containing 0.5 mM PMSF and 2.5 μM leupeptin. The pellet after ultracentrifugation at 100,000 g for 1 hour was resuspended in solubilization buffer (200 mM Tris-maleate, pH 6.5, 2 mM CaCl₂, 0.5 mM PMSF, 2.5 μM leupeptin, and 1% Triton X-100) as previously described (11). Conditioned medium was concentrated 20-fold using Centricon-100 concentrators (Millipore) (5). 50 ml of serum was purified using a RAP-GST affinity column. For immunoblotting, equal amounts of membrane protein, protein extracted from pelleted beads, or concentrated medium were subjected to 10% SDS-PAGE after heating to 95°C for 5 minutes as described (47) under reducing conditions and transferred to a nitrocellulose membrane. Incubations were with antibody against LR11 (5-4-30-19-2, 1:500 dilution; or pm11, 1:200 dilution), LRP1 (1:500 dilution) (phospho-) p44/42 MAP kinase (1:1000 dilution) (phospho-) Stat1 (1:500 dilution), Rac1 (1:1000 dilution), integrin αvβ3 (MAB1976, 1:1000 dilution), or uPAR (1:500 dilution) followed by peroxidase-conjugated anti-mouse, anti-rabbit, or anti-goat IgG. For immunoprecipitation, 100 μg of membrane protein was mixed with sLR11 (1 μg/μl) at 4°C for 3 hours in the presence or absence of apoE (50 μg) or RAP (10 μg), as indicated in Figure 6B. The LR11/uPAR/integrin/antibody complex was precipitated by protein A-Sepharose. The proteins were released into 25 μl SDS sample buffer by heating to 95°C for 5 minutes. For immunodetection, pm11 (1:200 dilution) was used, followed by peroxidase-conjugated anti-rabbit IgG. Development was performed with the ECL detection reagents (Amersham). The signals were quantified by densitometric scanning using NIH Image software. The sLR11 level of each subject's serum (50 μl) was determined in a blinded manner as an averaged value of 3 quantified signal
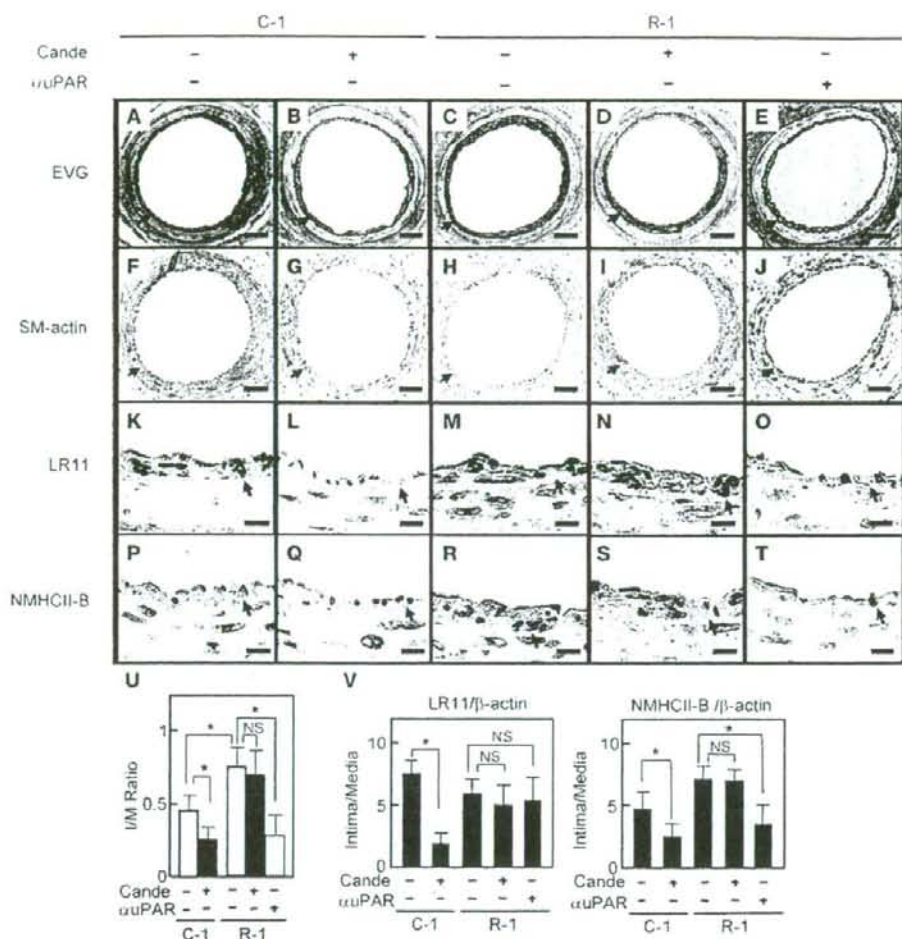
— 211 —

Figure 11
Effect of the ARB candesartan on intimal thickness after arterial injury in sLR11-overproducing mice. BL6 nude mice were implanted subcutaneously with A7r5 cells transfected with LR11 cDNA (R-1) or control cells (C-1). Sections of femoral arteries of cell-implanted mice after cuff placement with or without administration of candesartan or anti-uPAR neutralizing antibody were subjected to histological analysis using elastica van Gieson (EVG) staining (A–E). Serial sections were immunohistochemically analyzed using antibody against SMA (F–J), LR11 (K–O), or NMHCII-B (P–T). Arrowheads indicate the internal elastic layers. Scale bars: 50 μm (A–J); 10 μm (K–T). (U) I/M ratio of arteries is presented as mean ± SD (n = 5). *P < 0.05. (V) mRNA levels of LR11 and NMHCII-B in injured arteries. Total RNA isolated from thickened intima or media of mice using LCM was reverse transcribed and subjected to real-time PCR analysis using specific primers for NMHCII-B and LR11, respectively. The amounts of amplified products are expressed relative to the amounts of β-actin transcript, and the ratio of mRNA expression levels of intima and media are presented as mean ± SD (n = 3).

intensities resulting from independent assays and expressed as a ratio to that of a standard serum. The immunological estimation indicated that the signal of 1 U (in 50 μl serum) corresponded to approximately 50 ng/ml of recombinant sLR11. For analysis of phosphorylated ERK, Rac1 pull-down, and FAK phosphorylation, cells were starved for 24 hours in 0.3% FBS-DMEM followed by the addition of sLR11 (1 μg/ml) for the indicated times in the presence or absence of anti-integrin antibody (MAB1976 or RMV-7, 1:200 dilution) as described (13). For Rac1 pull-down and FAK phosphorylation assays, cells were lysed directly in the plates with ice-cold magnesium-containing lysis buffer and

RIPA buffer, respectively. GTP-Rac1 activity was measured with a PAK-1 PBD/ Rac activation assay kit (Upstate Biotechnology). In brief, lysates were incubated at 4°C with 10 μg of PAK-1 PBD Protein GST beads for 60 minutes. The proteins were released into 25 μl SDS sample buffer by heating to 95°C for 5 minutes. For FAK phosphorylation measurement after immunoprecipitation with antibody against FAK (MAb2A7), lysates were subjected to electrophoresis in 7.5% SDS gels and transferred to nitrocellulose membranes. The membranes were probed with an antibody specific for FAK-pY397 (1:1000) and then reprobed with an anti-FAK antibody (MAb2A7, 1:500).
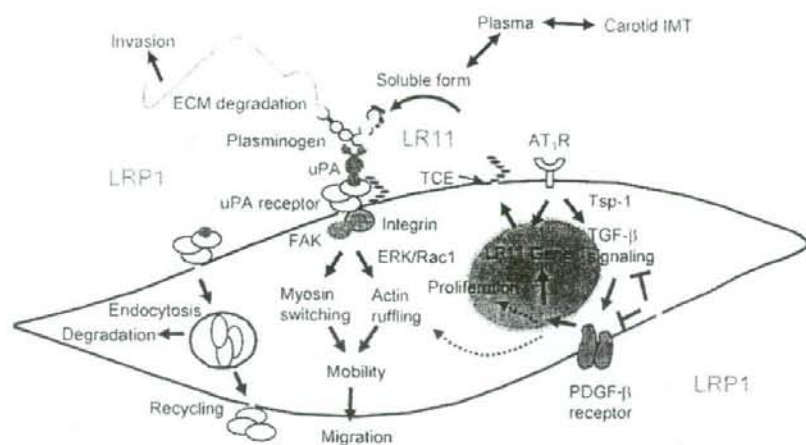
Figure 12

Proposed molecular mechanism for LR11 requirement in the response of SMCs to Ang II. Ang II and PDGF-BB are the key cytokines promoting migration of SMCs in plaque formation. LRP1 inhibits the PDGF-BB–mediated signals for migration and proliferation and/or the modulation of upstream Tsp-1/TGF-β–mediated signals (38) through interaction with the PDGF-β receptor. Ang II induces the Tsp-1/TGF-β signals (37) and LR11 gene transcription through activating AT₁R. LR11 localized on the cell surface becomes the soluble form (as sLR11) by cleavage through TNF-α–converting enzyme (TCE) (22). Circulating sLR11 levels are positively correlated with carotid IMT. sLR11 binds to and interacts with uPAR, the expression of which is mainly regulated by LRP1, on the cell surface and/or on neighboring cells. This complex formation inhibits the internalization of uPAR via LRP1, resulting in enhanced uPAR cell-surface expression. The uPA/uPAR system increases cell mobility through both increased ECM degradation and intracellular integrin/FAK/ERK/Rac-1 signaling, which in turn promotes actin ruffling and myosin isoform switching. The SMCs expressing LR11 display increased migratory capacity in response to PDGF-BB and/or Ang II. Thus, LR11 in combination with its counteracting partner LRP1 regulates the migration of intimal SMCs in injured arteries and atherosclerotic plaques via modulation of the uPA/uPAR system. The proposed LR11-mediated migration of intimal SMCs may be modulated by other Ang II–induced molecules and cytokines, particularly endothelial cell–derived PAI-1 (48). ARBs inhibit (a) the migration of intimal SMCs through downregulation of LR11 and (b) their proliferation by blockade of signals mediated by Tsp-1/TGF-β and PDGF-BB.

paraformaldehyde in PBS at 4°C for 15 minutes, as described (11). F-actin was labeled using Alexa Fluor 488 phalloidin (1:40 dilution, A12379; Invitrogen) for measurement of ruffle formation. Slides were examined with a Zeiss LSM5 PASCAL confocal laser scanning microscope. The 488-nm line of the argon laser was used for excitation of Alexa Fluor 488. The number of cells with membrane ruffling were counted with 500 cells in the field.

sLR11-overproducing mouse model. R-1 and C-1 cells were grown to near confluence, trypsinized, and suspended in DMEM with 10% FBS. After centrifugation, cell pellets were resuspended in PBS. Eight-week-old ICR nude mice were injected subcutaneously with either 1 × 10⁷ R-1 cells or C-1 cells. The injection through 21-gauge needles into subcutaneous areas of nude mice was performed under anesthesia, as described (23). The surgical operations for cuff placement and connection to a supply osmotic minipump for candesartan (0.1 mg/kg/day) followed 4 weeks after cell implantations. Polyclonal antibodies against uPAR (1:500 dilution) or against GST (control, 1:200 dilution) in PBS were injected intraperitoneally, in each case 2–3 days after cuff treatment of mice injected with R-1 cells. Blood samples were collected for the immunodetection of sLR11. Six weeks after cell implantation, the femoral arteries were recovered for immunohistological analyses.

Transfection of SMCs with siRNA. Oligonucleotides were synthesized for siRNA (Takara Bio Inc.). Annealed sense and antisense oligonucleotides (25 nM each), 5'-UGGCUUCCAAUGUUACAGCTT-3' and 5'-GCUGUAA-CAUUGGAAGCCATT-3' corresponding to the uPAR sequence, or 5'-GAUGC-CAUCUGUAGUCACUTT-3' and 5'-AGUGACUACAGAUGGCAUCTT-3' for control were transfected into SMCs (1 × 10⁶ cells/100 mm dish) and incubated for 2 days as described (14). Cells were then used for experiments.

Immunohistochemistry. Serial paraffin-embedded sections (5 μm) were used for immunohistostaining as described (11). Deparaffinized sections were pretreated with 0.3% H₂O₂ to inactivate endogenous peroxidase. Slides were stained in the presence of 3% BSA with antibody against LR11 (pm11, 1:50 dilution), NMHCII-B (1:100 dilution), or SMA (1:1 dilution) at 23°C for 1 hour followed by HRP-conjugated anti-rabbit IgG secondary antibodies (Molecular Probes) at 1:200 dilution. The slides were counterstained with hematoxylin. Controls with nonimmune rabbit IgG were conducted in parallel with each immunoassay procedure.

Immunofluorescence. Cells were grown to 70% confluence on LabTek chamber slides (Nunc). For assays of membrane ruffling, cells were preincubated with PDGF-BB (10 ng/ml), Ang II (1 μM), sLR11 (1 μg/ml), anti-LR11 antibody (pm11, 1:5 dilution), anti-uPAR antibody (10 μg/ml), anti-integrin αvβ3 antibody (10 μg/ml), or PD98059 (10 μM; Calbiochem) for the indicated times. Cells were fixed in 4%

PBS were injected intraperitoneally, in each case 2–3 days after cuff treatment of mice injected with R-1 cells. Blood samples were collected for the immunodetection of sLR11. Six weeks after cell implantation, the femoral arteries were recovered for immunohistological analyses.

Statistics. Statistical analysis was performed with SPSS version 13.0 (SPSS Japan Inc.). Associations of IMT or sLR11 levels with risk factors were examined by Pearson correlation analysis for continuous variables and by unpaired *t* test for categorical variables between groups (sex and smoking) (see Supplemental Table 2). Subsequently, multiple linear regression analyses were used to calculate the ORs for the IMT for Table 1 (a) by controlling for age, blood pressure, and HDL-C, which are significantly correlated with IMT, with $P < 0.001$ by above analyses (model 1); and (b) by additionally controlling for all risk factors (age, sex, BMI, blood pressure, smoking, LDL-C, HDL-C, triglycerides, LDL size, malondialdehyde-LDL, glucose, and insulin) used for the above analyses (model 2). Finally, the ORs were calculated for the IMT with raised baseline sLR11 (second, third, and fourth quartiles) compared with low baseline sLR11 (lowest quartile) by controlling for age. In the figures, the results are shown as mean ± SD for each index. 1-way ANOVA was used to compare between 2 groups, and Duncan's multiple-range test was used for comparison of multiple groups. A value of $P < 0.05$ was considered significant.

1. Ross, R. 1999. Atherosclerosis — an inflammatory disease. *N. Engl. J. Med.* **340**:115–126.
2. Newby, A.C. 2005. Dual role of matrix metalloproteinases (matrixins) in intimal thickening and atherosclerotic plaque rupture. *Physiol. Rev.* **85**:1–31.
3. Blasi, F., and Carmeliet, P. 2002. uPAR: a versatile signalling orchestrator. *Nat. Rev. Mol. Cell. Biol.* **3**:932–943.
4. Reuning, U., Magdolen, V., Hapke, S., and Schmitt, M. 2003. Molecular and functional interdependence of the urokinase-type plasminogen activator system with integrins. *Biol. Chem.* **384**:1119–1131.
5. Herz, J., and Hui, D.Y. 2004. Lipoprotein receptors in the vascular wall. *Curr. Opin. Lipidol.* **15**:175–181.
6. Gonias, S.L., Wu, L., and Salicioni, A.M. 2004. Low density lipoprotein receptor-related protein: regulation of the plasma membrane proteome. *Thromb. Haemost.* **91**:1056–1064.
7. Bujo, H., and Saito, Y. 2006. Modulation of smooth muscle cell migration by members of the low-density lipoprotein receptor family. *Arterioscler. Thromb. Vasc. Biol.* **26**:1246–1252.
8. Yamazaki, H., et al. 1996. Elements of neural adhesion molecules and a yeast vacuolar protein sorting receptor are present in a novel mammalian low density lipoprotein receptor family member. *J. Biol. Chem.* **271**:24761–24768.
9. Jacobsen, L. et al. 1996. Molecular characterization of a novel human hybrid-type receptor that binds the α₂-macroglobulin receptor associated protein (RAP). *J. Biol. Chem.* **271**:31379–31383.
10. Morwald, S., et al. 1997. A novel mosaic protein containing LDL receptor elements is highly conserved in humans and chickens. *Arterioscler. Thromb. Vasc. Biol.* **17**:996–1002.
11. Zhu, Y., et al. 2004. LR11, an LDL receptor gene family member, is a novel regulator of smooth muscle cell migration. *Circ. Res.* **94**:752–758.
12. Kanaki, T., et al. 1999. Expression of LR11, a mosaic LDL receptor family member, is markedly increased in atherosclerotic lesions. *Arterioscler. Thromb. Vasc. Biol.* **19**:2687–2695.
13. Zhu, Y., et al. 2002. Enhanced expression of the LDL receptor family member LR11 increases migration of smooth muscle cells in vitro. *Circulation.* **105**:1830–1836.
14. Jiang, M., et al. 2006. Pitavastatin attenuates the PDGF-induced LR11/uPA receptor-mediated migration of smooth muscle cells. *Biochem. Biophys. Res. Commun.* **348**:1367–1377.
15. Xi, X.P., et al. 1999. Central role of the MAPK pathway in rat vascular smooth muscle cells. *Arterioscler. Thromb. Vasc. Biol.* **19**:73–82.
16. Nickenig, G., and Harrison, D.G. 2002. The AT₁-type angiotensin receptor in oxidative stress and atherogenesis: part I: oxidative stress and atherogenesis. *Circulation.* **105**:393–396.
17. Zuo, L., et al. 2005. Caveolin-1 is essential for activation of Rac1 and NAD(P)H oxidase after angiotensin II type 1 receptor stimulation in vascular smooth muscle cells: role in redox signaling and vascular hypertrophy. *Arterioscler. Thromb. Vasc. Biol.* **25**:1824–1830.

18. Horiuchi, M., et al. 2003. Fluvastatin enhances the inhibitory effects of a selective angiotensin II type 1 receptor blocker, valsartan, on vascular neointimal formation. *Circulation.* **107**:106–112.
19. O'Leary, D.H., et al. 1999. Carotid-artery intima and media thickness as a risk factor for myocardial infarction and stroke in older adults. Cardiovascular Health Study Collaborative Research Group. *N. Engl. J. Med.* **340**:14–22.
20. Ohwaki, K., et al. 2007. A secreted soluble form of LR11, specifically expressed in intimal smooth muscle cells, accelerates formation of lipid-laden macrophages. *Arterioscler. Thromb. Vasc. Biol.* **27**:1050–1056.
21. Manabe, I., and Nagai, R. 2003. Regulation of smooth muscle phenotype. *Curr. Atheroscler. Rep.* **5**:214–222.
22. Hermey, G., Sjogaard, S.S., Petersen, C.M., Nykjaer, A., and Gliemann, J. 2006. Tumour necrosis factor alpha-converting enzyme mediates ectodomain shedding of Vps10p-domain receptor family members. *Biochem. J.* **395**:285–293.
23. Kitagawa, Y., et al. 2004 Impaired glucose tolerance is accompanied by decreased insulin sensitivity in tissues of mice implanted with cells that overexpress resistin. *Diabetologia.* **47**:1847–1853.
24. Trommsdorff, M., et al. 1999. Reeler/Disabled-like disruption of neuronal migration in knockout mice lacking the VLDL receptor and ApoE receptor 2. *Cell.* **97**:689–701.
25. Webb, D.J., Nguyen, D.H.D., Sankovic, M., and Gonias, S.L. 1999. The very low density lipoprotein receptor regulates urokinase receptor catabolism and breast cancer cell motility in vitro. *J. Biol. Chem.* **274**:7412–7420.
26. Webb, D.J., Nguyen, D.H.D., and Gonias, S.L. 2000. Extracellular signal-regulated kinase functions in the urokinase receptor-dependent pathway by which neutralization of low density lipoprotein receptor-related protein promotes fibrosarcoma cell migration and matrigel invasion. *J. Cell Sci.* **113**:123–134.
27. Ma, Z., et al. 2002. Regulation of Rac1 activation by the low density lipoprotein receptor-related protein. *J. Cell Biol.* **159**:1061–1070.
28. Zhu, Y., and Hui, D.Y. 2002. Low density lipoprotein receptor-related protein mediates apolipoprotein E inhibition of smooth muscle cell migration. *J. Biol. Chem.* **277**:4141–4146.
29. Boucher, P., Gotthardt, M., Li, W.P., Anderson, R.G., and Herz, J. 2003. LRP: role in vascular wall integrity and protection from atherosclerosis. *Science.* **300**:329–332.
30. Swertfeger, D.K., Bu, G., and Hui, D.Y. 2003. Apolipoprotein E binding to low density lipoprotein receptor-related protein-1 inhibits cell migration via activation of cAMP-dependent protein kinase A. *J. Biol. Chem.* **278**:36257–36263.
31. Orr, A.W., Elzie, C.A., Kucik, D.F., and Murphy-Ullrich, J.E. 2003. Thrombospondin signaling through the calreticulin/LDL receptor-related protein co-complex stimulates random and directed cell migration. *J. Cell Sci.* **116**:2917–2927.
32. Tanaga, K., et al. 2004. LR11 attenuates the migration of smooth muscle cells by reducing membrane localization of urokinase and PDGF receptors.

Arterioscler. Thromb. Vasc. Biol. **24**:1422–1428.
33. Seki, N., et al. 2005. LRP1B is a negative modulator of increased migration activity of intimal smooth muscle cells from rabbit aortic plaques. *Biochem. Biophys. Res. Commun.* **331**:964–970.
34. Nykjaer, A., et al. 1997. Recycling of the urokinase receptor upon internalization of the uPA:serpin complexes. *EMBO J.* **16**:2610–2620.
35. Liu, C.X., et al. 2001. The putative tumor suppressor LRP1B, a novel member of the low density lipoprotein (LDL) receptor family, exhibits both overlapping and distinct properties with the LDL receptor-related protein. *J. Biol. Chem.* **276**:28889–28896.
36. Degryse, B., et al. 2001. Urokinase/urokinase receptor and vitronectin/alpha(v)beta(3) integrin induce chemotaxis and cytoskeleton reorganization through different signaling pathways. *Oncogene.* **20**:2032–2043.
37. Cohn, R.D., et al. 2007. Angiotensin II type 1 receptor blockade attenuates TGF-beta-induced failure of muscle regeneration in multiple myopathic states. *Nat. Med.* **13**:204–210.
38. Boucher, P., et al. 2007. LRP1 functions as an atheroprotective integrator of TGFbeta and PDGF signals in the vascular wall: implications for Marfan syndrome. *PLoS ONE.* **2**:e448.
39. Rogaeva, E., et al. 2007. The neuronal sortilin-related receptor SORL1 is genetically associated with Alzheimer disease. *Nat. Genet.* **39**:168–177.
40. Scherzer, C.R., et al. 2004. Loss of apolipoprotein E receptor LR11 in Alzheimer disease. *Arch. Neurol.* **61**:1200–1205.
41. Sagare, A., et al. 2007. Clearance of amyloid-beta by circulating lipoprotein receptors. *Nat. Med.* **13**:1029–1031.
42. Fujita, Y., et al. 2005. Association of nucleotide variations in the apolipoprotein B48 receptor gene (APOB48R) with hypercholesterolemia. *J. Hum. Genet.* **50**:203–209.
43. Taira, K., et al. 2002. Positive family history for coronary heart disease and 'midband lipoproteins' are potential risk factors of carotid atherosclerosis in familial hypercholesterolemia. *Atherosclerosis.* **160**:391–397.
44. Bujo, H., et al. 1994. Chicken oocyte growth is mediated by an eight ligand binding repeat member of the LDL receptor family. *EMBO J.* **13**:5165–5175.
45. Kobayashi, K., et al. 2005. Targeted disruption of TGF-beta-Smad3 signaling leads to enhanced neointimal hyperplasia with diminished matrix deposition in response to vascular injury. *Circ. Res.* **96**:904–912.
46. Hirata, T., Unoki, H., Bujo, H., Ueno, K., and Saito, Y. 2006. Activation of diacylglycerol O-acyltransferase 1 gene results in increased tumor necrosis factor-alpha gene expression in 3T3-L1 adipocytes. *FEBS Lett.* **580**:5117–5121.
47. Bujo, H., et al. 1995. Mutant oocytic low density lipoprotein receptor gene family member causes atherosclerosis and female sterility. *Proc. Natl. Acad. Sci. U. S. A.* **92**:9905–9909.
48. Redmond, E.M., et al. 2001. Endothelial cells inhibit flow-induced smooth muscle cell migration: role of plasminogen activator inhibitor-1. *Circulation.* **103**:597–603.

— 214 —

Matrix Metalloproteinase-3 Enhances the Free Fatty Acids-Induced VEGF Expression in Adipocytes Through Toll-Like Receptor 2

Toru Kawamura,* Kentaro Murakami,* Hideaki Bujo,†[1] Hiroyuki Unoki,‡
Meizi Jiang,† Toshinori Nakayama,§ and Yasushi Saito*

*Department of Clinical Cell Biology, †Department of Genome Research and Clinical Application,
‡Department of Applied Translation Research, and §Department of Immunology, Chiba University
Graduate School of Medicine, Chuo-ku, Chiba 260-8670, Japan

Infiltrated macrophages (Mφ) are believed to cause pathological changes in the surrounding adipocytes through the secretion of active molecules in visceral fat. Matrix metalloproteinase (MMP)-3 is secreted from Mφ, and enhances expression of the inflammatory cytokines through the activation of toll-like receptor (TLR) 2. Visceral adipocytes express high levels of vascular endothelial growth factor (VEGF), and the degree of visceral fat accumulation is associated with the plasma VEGF concentration in obese subjects. The aim of the study is to clarify the role of MMP-3 in the enhancement of the free fatty acids (FFAs)-induced VEGF expression through TLR2 in visceral adipocytes. One mM FFAs induced VEGF mRNA and protein expression in 3T3-L1 adipocytes. The FFAs-induced VEGF expression was mostly mediated by TLR2. A high fat intake increased the VEGF mRNA expression in visceral fat and the VEGF concentration in plasma, accompanied with the increase in the plasma FFAs concentration in mice. These increases were largely inhibited in TLR2-deficient mice. The FFAs-induced VEGF expression was increased in the presence of Mφ-conditioned medium (CM) in adipocytes, and the enhancement was inhibited by a MMP-3 inhibitor or a neutralizing antibody against MMP-3. The active form of MMP-3 induced the VEGF mRNA expression, as well as TLR2, in adipocytes. The increase in the VEGF expression by MMP-3 was inhibited by the treatment with siRNA for TLR2. The enhancement of FFAs-induced TLR2 expression by Mφ-CM was inhibited by blocking of the MMP-3. The increase in the VEGF mRNA expression by Mφ-CM or MMP-3 was partially inhibited by a neutralizing

antibody against TNF-α. These results indicate that MMP-3 in Mφ-CM enhances the FFAs-induced VEGF expression in adipocytes through the increase in the TLR2 expression. The MMP-3 secreted from the infiltrated Mφ may be a regulator of the VEGF expression in visceral adipocytes. Exp Biol Med 233:1213–1221, 2008

Key words: matrix metalloproteinase-3; toll-like receptor 2; macrophage; vascular endothelial growth factor; adipocyte; visceral fat

Introduction

Adipocytes secrete a wide variety of cytokines, and some cause metabolic disturbance through the development of insulin resistance (1–3). The expression of toll-like receptor (TLR) 2 gene is associated with the gene expression of TNF-α (4), one of the cytokines that causes an inhibition of insulin signals in fat, muscle and liver (1–3, 5). High fat feeding leads to an increased population of TLR2/TNF-α co-expressing adipocytes in visceral fat, but not in subcutaneous fat in mice (4). A microarray analysis revealed that the accumulated visceral fat is accompanied with drastic changes in expression of matrix metalloproteinase (MMP) family genes, among which MMP-3 potentiated free fatty acids (FFAs)-induced TNF-α secretion from adipocytes (6). Infiltrated macrophage (Mφ) has a potential for a pathological link with surrounding adipocytes through the secretion of MMP-3 followed by TNF-α expression in adipocytes in visceral fat tissue (7).

Vascular endothelial growth factor (VEGF) is abundantly secreted from adipocytes, and it plays a key role in the process of fat tissue formation through the regulation of angiogenesis in the tissues (8). The inhibition of angiogenesis leads to a decreased volume of developing fat tissue or fat grafting after transplantation in mice (9, 10). VEGF is highly expressed in visceral fat, and the circulating VEGF concentration is positively correlated with visceral fat

1213

volume in obese mice (11). These observations suggest that the TLR2 expression in adipocytes is related to the expression of VEGF as well as TNF-α. In this context, the tight association between visceral fat accumulation and the plasma VEGF level is in fact observed in obese human subjects (12). However, the mechanism for the induction of VEGF expression in visceral fat has not been elucidated.

FFAs have been shown to activate the downstream signals of TLR2 (13, 14). The aim of this study was to clarify the role of MMP-3 in the enhancement of the FFAs-induced VEGF expression through TLR2 in visceral adipocytes. The significance of TLR2 for the FFAs-induced VEGF expression was at first analyzed in cultured adipocytes and the visceral fat of TLR2-deficient mice. Next, the possible pathological role of the MMP-3 secreted from Mφ in the FFAs-induced VEGF expression through TLR2 was assessed in a culture system using conditioned medium (CM) of Mφ.

Materials and Methods

Adipocyte Culture. 3T3-L1 preadipocytes (American Type Culture Collection, Rockville, MD) were cultured in high-glucose DMEM (DMEM-H, GibcoBRL, Tokyo, Japan) supplemented with 10% FBS (Sigma, St. Louis, MO) and antibiotics. After the 3T3-L1 preadipocytes were grown to near confluence, the differentiation to mature adipocytes was performed using insulin (Sigma), dexamethasone (Sigma), and 3-isobutyl-1-methyl-xanthine (Sigma), as described previously (7). A vast majority of cells (~90%) had accumulated lipid droplets between 10–14 days after differentiation and were used for further experiments.

Cell Treatment with FFAs. The treatment of 3T3-L1 cells with FFAs was performed essentially according to the method previously described (15). After overnight incubation in serum-free DMEM-H supplemented with 0.1% FFAs-free BSA, the cells were treated in serum-free DMEM-H supplemented with 0.1% FFAs-free BSA with 1 mM FFAs (a cocktail containing 0.5 mM palmitic acid and 0.5 mM myristic acid, Sigma) for indicated times, and then incubated in serum-free DMEM-H supplemented with 0.1% FFAs-free BSA with 1 mM FFAs in the presence or absence of 1 μg/ml zymosan A (Wako, Tokyo, Japan), 10 μg/ml peptidoglycan (PGN, Invitrogen, Tokyo, Japan), or 100 μg/ml active form of MMP-3 purified from human fibroblasts (Sigma), a neutralizing antibody against TNF-α (15) (R&D Systems, Minneapolis, MN) or non-immune IgG (R&D Systems) for indicated times. The composition ratio of FFAs/BSA in the medium corresponds to 6:1 for the first incubation medium.

Quantitative Real-Time Reverse Transcriptase-Polymerase Chain Relation (RT-PCR). Total RNA was extracted from fat tissue or 3T3-L1 adipocytes using RNeasy Mini kit (QIAGEN, Valencia, CA), and was reverse transcribed using the GeneAmp Gold RNA PCR Reagent kit (PE Applied Biosystems, Foster City, CA) as described previously (7). Quantitative RT-PCR amplifications were performed using TaqMan Universal PCR Master Mix and Assay-on-Demand Gene expression Assay Mix specific for mouse VEGF A (Mm000437304_m1) or TLR2 (Mm00442346_m1) mRNA. All PCRs were performed in an ABI PRISM 7500 sequence detection system (PE Applied Biosystems).

Enzyme-Linked Immunosorbent Assay (ELISA). The VEGF concentration of plasma or cell culture medium was measured using a Quantikine Mouse VEGF Immunoassay kit (R&D Systems).

siRNA Knockdown Treatment. 3T3-L1 adipocytes or THP-1-derived Mφ were transfected either with 5 nmol siRNA for TLR2 (QIAGEN) or MMP-3 (Invitrogen), or Allstars Negative Control (QIAGEN) siRNA by electroporation as described previously (7). The cells were reseeded after electroporation, and incubated with DMEM-H containing 10% FBS for two days. After overnight incubation in serum-free DMEM-H supplemented with 0.1% FFA-free BSA, the siRNA-treated 3T3-L1 adipocytes were incubated in serum-free DMEM-H supplemented with 0.1% FFA-free BSA and 1 mM FFAs for 6 h. The CM of the siRNA-treated Mφ was prepared by the incubation for the following 24 h.

Mice. TLR2$^{-/-}$ mice were kindly provided by Dr. Shizuo Akira (Osaka University) (16). Briefly, mouse TLR2 gene was disrupted by introducing a targeted mutation into E14.1 embryonic stem cells. A targeting vector was designed to replace a part of the exon that encodes the transmembrane and the cytoplasmic domain of TLR2 with the *neo* gene. ES cell lines containing a mutant TLR2 allele were microinjected into C57BL/6 blastocysts. Heterozygous mice were intercrossed to produce TLR2$^{-/-}$ mice and TLR2$^{+/+}$ mice. The TLR2$^{-/-}$ mice grew healthy and did not show any obvious abnormality until 20 weeks. TLR2 mRNA could not be detected in either the mesenteric or subcutaneous fat tissue of the TLR2$^{-/-}$ mice. From five weeks of age, female TLR2$^{+/+}$ and TLR2$^{-/-}$ mice were given either a regular (D12450B, Research Diet, New Brunswick, NJ, see Table 1) or a high fat diet (D12492).

Preparation of Mφ-CM. The preparation of Mφ-CM was performed essentially as described (7). The human monocytic cell line THP-1 (American Type Culture Collection) was cultured in RPMI 1640 supplemented with l-glutamine (GibcoBRL) and antibiotics and 10% FBS. To allow the monocytes to differentiate into adherent macrophages, THP-1 cells were washed in PBS (calcium- and magnesium-free, GibcoBRL, medium A) and re-suspended in fresh medium A containing 50 ng/ml phorbol 12-myristate–13-acetate (PMA, Sigma) for 3 days (at day 0). The cells were incubated for 3 more days in DMEM supplemented with 2% BSA, and then at day 4, the cells were treated for the CM preparation for 24 h. Control CM was prepared by incubating the THP-1 cells without the differentiation treatment (THP1-CM).

Treatment of Adipocytes with Mφ-CM. After treatment in serum-free DMEM-H supplemented with

Table 1.   Contents of Regular and High Fat Diets

	Regular diet (D12450B)		High fat diet (D12492)	
	g %	kcal %	g %	kcal %
Protein	19.2	20	26.2	20
Carbohydrate	67.3	70	26.3	20
Fat	4.3	10	34.9	60
Total		100		100
kcal/g	3.85		5.24	
	g	kcal	g	kcal
Casein, 80 mesh	200	800	200	800
L-Cystine	3	12	3	12
Corn starch	315	1260	0	0
Maltodextrin 10	35	140	125	500
Sucrose	350	1400	68.8	275.2
Cellulose, BW200	50	0	50	0
Soybean oil	25	225	25	225
Lard	20	180	245	2205
Mineral mix S10026	10	0	10	0
DiCalcium phosphate	13	0	13	0
Calcium carbonate	5.5	0	5.5	0
Potassium citrate, 1 H2O	16.5	0	16.5	0
Vitamin mix V10001	10	40	10	40
Choline bitartrate	2	0	2	0
Total	1055.05	4057	773.85	4075

0.1% FFA-free BSA and 1 mM FFAs for 6 h, 3T3-L1 adipocytes were incubated in serum-free DMEM-H supplemented with 0.1% FFA-free BSA and 1 mM FFAs with Mφ-CM or THP1-CM at 10% of the final volume, or the active form of MMP-3 for the indicated time periods. Mφ-CM or THP1-CM was treated with an MMP-3 inhibitor, NNGH (*N*-isobutyl-*N*-(4-methoxyphenylsulfonyl)-glycylhydroxamic acid; Calbiochem, San Diego, CA) (17, 18), goat anti-MMP-3 polyclonal antibody (Santa Cruz, Santa Cruz, CA) or non-immune goat IgG (Santa Cruz) for 12 h, prior to the addition to adipocytes.

Statistical Analyses. The results are presented as the mean ± SD. Statistical significance between two groups was evaluated by Student's *t*-test. Statistical significance among several groups was performed using a one-way ANOVA. A value of $P < 0.05$ was considered to be significant.

Results

FFAs-Induced VEGF mRNA Expression Is Mediated by TLR2 in 3T3-L1 Adipocytes. FFAs induce the TNF-α expression through the increased TLR2 expression in adipocytes (4). The effect of FFAs on the expression of VEGF mRNA through TLR2 was analyzed in 3T3-L1 adipocytes. The VEGF mRNA expression levels were increased time-dependently in the presence of 1 mM FFAs (a cocktail containing 0.5 mM palmitic acid and 0.5 mM myristic acid) (Fig. 1A). The VEGF concentration in the medium for 72 hr after incubation of 3T3-L1 adipocytes in the presence of 1 mM FFAs was significantly higher than that in the absence of FFAs (Fig. 1B). Zymosan A, a TLR2

ligand that induces the TNF-α mRNA expression in 3T3-L1 adipocytes (4, 19), showed the effect additive to the treatment with FFAs on the increase in the VEGF mRNA expression in the cells (Fig. 1C). Furthermore, the VEGF mRNA expression was increased to 1.8-fold by 10 g/ml peptidoglycan (PGN), another TLR2 ligand (19), in comparison to that without the addition in the cells incubated with FFAs (data not shown). The FFAs-induced increase in the VEGF mRNA expression level was mostly abolished in the adipocytes transfected with TLR2-specific siRNA in comparison to that in the cells transfected with control siRNA (Fig. 1D). These results indicate that FFAs-induced VEGF mRNA expression is most likely mediated by TLR2 in 3T3-L1 adipocytes.

A High Fat Intake Increases the VEGF mRNA Expression in Visceral Fat, Accompanied with an Increase in Plasma VEGF Concentration in TLR2$^{+/+}$ Mice, but Not in TLR2$^{-/-}$ Mice. The above observations for the FFAs-induced VEGF expression through TLR2 in cultured adipocytes suggest that a high fat intake may induce the VEGF mRNA expression through the FFAs-mediated TLR2 expression in fat tissues. The expression levels of VEGF mRNA in the fat tissues of TLR2$^{+/+}$ mice and TLR2$^{-/-}$ mice were investigated after fat feeding for six weeks. Plasma FFAs levels were significantly increased in the high fat-fed TLR2$^{+/+}$ mice in comparison to those in the regular diet-fed TLR2$^{+/+}$ mice, and were not significantly different from the high fat-fed TLR2$^{-/-}$ mice (Fig. 2A). The expression levels of VEGF mRNA in mesenteric fat were significantly increased in the high fat-fed TLR2$^{+/+}$ mice in comparison to those in regular
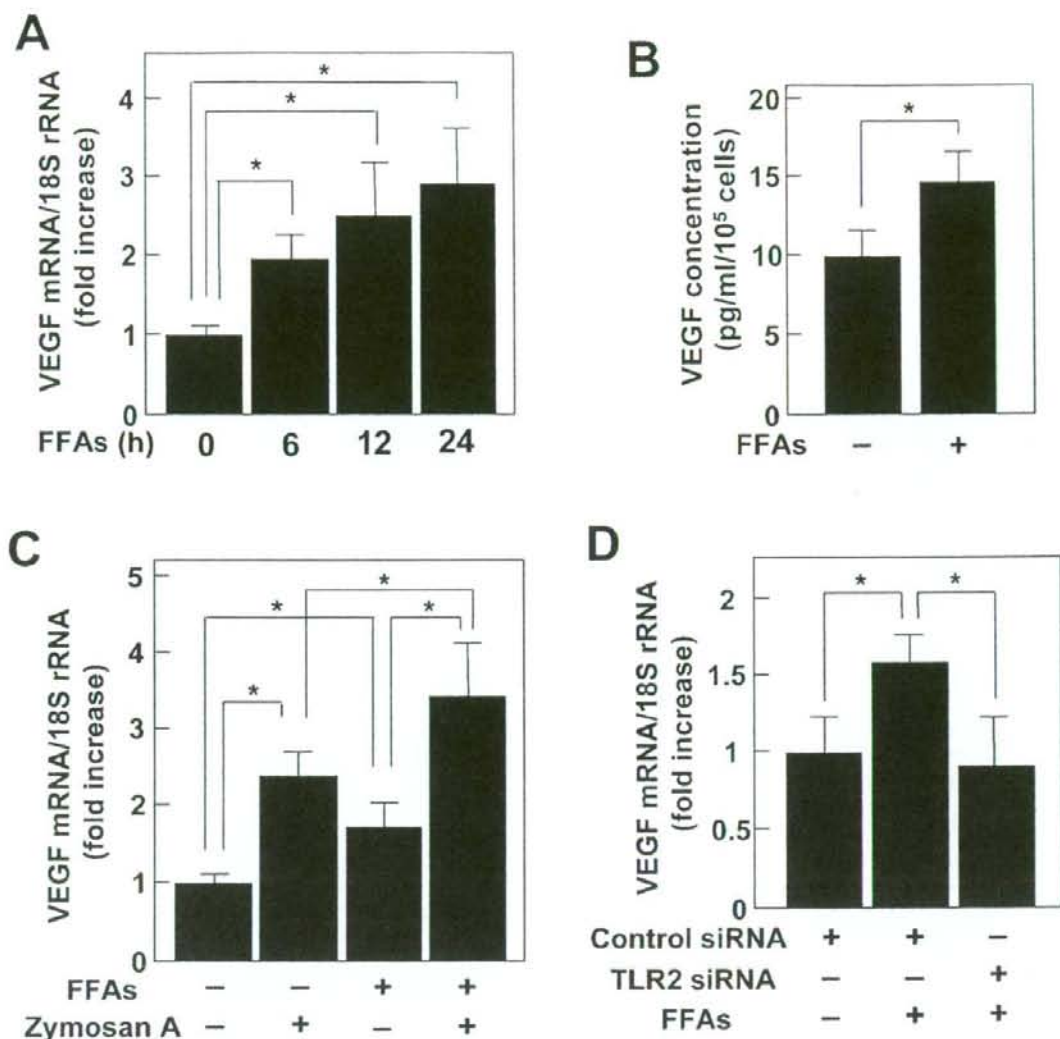
Figure 1. The effect of FFAs with zymosan A or TLR2 knockdown on the VEGF expression in 3T3-L1 adipocytes. (A) Total RNA was extracted from adipocytes after incubation with 1 mM FFAs (a cocktail of 0.5 mM palmitic acid and 0.5 mM myristic acid) for indicated time. The VEGF mRNA level was evaluated by quantitative real-time RT-PCR. mRNA levels were calculated as the fold increase of the control at 0 h. The bars represent the mean ± SD ($n = 3$). * $P < 0.05$. (B) Conditioned media were collected after incubation of adipocytes with 1 mM FFAs for 72 h. The VEGF concentration was measured using ELISA, and then presented by the correction with the incubated cell number. The cell appearance was not changed after the incubation with FFAs, and no significant difference was observed in the cell counts between the adipocytes incubated with and without FFAs. The bars represent the mean ± SD ($n = 3$). * $P < 0.05$. (C) Adipocytes were incubated with or without 1 mM FFAs for 6 h, and then with or without 1 mM FFAs in the presence or absence of 1 μg/ml Zymosan A for 6 h. Total RNA was extracted from adipocytes, and the VEGF mRNA level was evaluated by quantitative real-time RT-PCR. The mRNA levels were calculated as the fold increase of the control in the absence of FFAs or zymosan A. The bars represent the mean ± SD ($n = 3$). * $P < 0.05$. (D) Adipocytes were transfected either with TLR2-specific siRNA or control siRNA. Total RNA was extracted from the adipocytes after incubation with or without 1 mM FFA for 6 h. The mRNA levels were calculated as the fold increase of those of cells transfected with control siRNA without the FFA treatment. The bars represent the mean ± SD ($n = 5$). * $P < 0.05$.